

# The Space of Adversarial Strategies

Ryan Sheatsley\*  
*University of Wisconsin-Madison*

Eric Pauley  
*University of Wisconsin-Madison*

Blaine Hoak\*  
*University of Wisconsin-Madison*

Patrick McDaniel  
*University of Wisconsin-Madison*

## Abstract

*Adversarial examples*, inputs designed to induce worst-case behavior in machine learning models, have been extensively studied over the past decade. Yet, our understanding of this phenomenon stems from a rather fragmented pool of knowledge; at present, there are a handful of attacks, each with disparate assumptions in threat models and incomparable definitions of optimality. In this paper, we propose a systematic approach to characterize worst-case (i.e., optimal) adversaries. We first introduce an extensible decomposition of attacks in adversarial machine learning by atomizing attack components into *surfaces* and *travelers*. With our decomposition, we enumerate over components to create 576 attacks (568 of which were previously unexplored). Next, we propose the Pareto Ensemble Attack (PEA): a theoretical attack that upper-bounds attack performance. With our new attacks, we measure performance relative to the PEA on: both robust and non-robust models, seven datasets, and three extended  $\ell_p$ -based threat models incorporating compute costs, formalizing the *Space of Adversarial Strategies*. From our evaluation we find that attack performance to be highly contextual: the domain, model robustness, and threat model can have a profound influence on attack efficacy. Our investigation suggests that future studies measuring the security of machine learning should: (1) be contextualized to the domain & threat models, and (2) go beyond the handful of known attacks used today.

## 1 Introduction

It is well-known that machine learning models are vulnerable to *adversarial examples*—inputs designed to induce worst-case behavior. Seminal papers have introduced a suite of varying techniques for producing adversarial examples, each with their own unique threat models, strengths, and weaknesses [7, 22, 33, 35, 39]. Every generation of research yields the next evolution of attacks, designed to overcome prior defenses. It is unclear whether this evolution will ever converge,

yet it is apparent that there are some attacks that have “survived” modern defenses. Specifically, the accepted baselines for evaluating defenses are converging to a small set of largely fixed attacks and threat models.

This observation on the fixed nature of commonly used attacks speaks to a broader and more fundamental problem in the way we evaluate the trustworthiness of machine learning systems: our understanding of adversaries has been derived from a union of works with disjoint assumptions and underlying threat models. As a consequence, it is challenging to draw any universal truths from a rather fragmented (and broadly incomparable) pool of knowledge. Subsequently, comparisons between attacks and attempts at characterizing *the* worst-case adversary have been through the lens of a specific threat model and defined with respect to a small handful of attacks, making it difficult to discern the true strength of claims on what is good (or even best) and when.

In this paper, we introduce a systematic approach to determine worst-case adversaries. We first introduce 568 new attacks by anatomizing seminal attacks into interchangeable components, therein enabling a meaningful evaluation of model robustness against an expansive attack space. With this decomposition, we formalize an extensible *Space of Adversarial Strategies*: the set of attacks considered by an adversary under a specific threat model and domain. We then empirically approximate the Pareto Ensemble Attack (PEA): a theoretical attack which upper-bounds attack performance by returning the optimal set of adversarial examples for a given threat model and dataset. We then use the PEA to explore a fundamental question: *Does an optimal attack exist?*

Our analysis begins by decomposing seminal attacks in adversarial machine learning. We observe that all known attacks are broadly built from two components: (1) a *surface*, and (2) a *traveler*. Surfaces encode the traversable attack space (often as the gradient of a cost function), while travelers are “vehicles” that navigate a surface to meet adversarial goals. Attack components live within surfaces and travelers, which characterize attack behavior, such as building crude surfaces that favor meeting adversarial goals without regard to budget,

\*Equal contribution

or vice-versa. Our decomposition allows us to (a) generalize attacks in an extensible manner, and (b) naturally construct new (and known) attacks by permuting attack components.

From our decomposition, we permute attack components to build a previously unexplored attack space, yielding 568 new attacks. We then measure attack performance through the PEA, which is built by forming the *lower envelope* of measured model accuracy across attacks over the budget consumed. In other words, the PEA bounds the performance an individual attack could achieve. We rank attacks with respect to the PEA by measuring the difference in areas of their performance curves. Our approach not only gives us a comparable definition of optimality, but also a mechanism by which we can measure the merit of individual attacks.

Our evaluation across seven datasets, three threat models, and robust (through adversarial training) versus non-robust models found relative attack performance to be highly contextual. Specifically, (1) the domain and threat model can have a profound effect (especially if the trained model is robust), and (2) even the advantage of certain component choices is sensitive to these factors, as well as other paired components. We make the following contributions:

- We propose a decomposition of attacks in adversarial machine learning by atomizing attack components into two main layers, *surfaces* and *travelers*. Our decomposition readily enables extensions of new components.
- We characterize the attack space by permuting components of known attacks, yielding 568 new attacks.
- We introduce a systematic approach to compare the efficacy of attacks. We first build the Pareto Ensemble Attack from the performance curves of attacks and rank their relative performance.
- We instantiate and enumerate over a hypothesis space to identify which strategies perform better than others under a given threat model.

## 2 Background

### 2.1 Threat Models

Adversaries have historically had one of two goals: minimizing model accuracy [32, 35, 39, 53] or maximizing model loss [3, 22, 33]. The risks associated with minimizing model accuracy are often exemplified by vehicles misclassifying traffic signs [19], intrusion detection systems permitting malicious entities entry [59], medical misdiagnoses [20], among other failures. Maximizing model loss serves two purposes: (1) it is a surrogate for minimizing model accuracy (as, the inverse is performed to maximize model accuracy during model training), and (2) it aids in transferability attacks [18, 37, 38, 55]. In this work, we focus on minimizing model accuracy and defer the explorations of transferability to future work.

In the context of minimizing model accuracy, translating the risks above into an optimization objective to be solved by an adversary is commonly written as:

$$\begin{aligned} \arg \min_{\epsilon} \quad & \|\epsilon\|_p \\ \text{subject to} \quad & f(x + \epsilon) \neq \hat{y}, \\ & x + \epsilon \in \mathcal{B}_\phi(x). \end{aligned} \tag{1}$$

where we are given a victim model  $f$ , a sample  $x$ , label  $\hat{y}$ , a self-imposed budget  $\phi$  measured under some  $\ell_p$ -norm. Conceptually, the adversary searches within some self-imposed norm-ball  $\mathcal{B}$  of radius  $\phi$ , centered at  $x$  for a “small” change  $\epsilon$  that, when applied to  $x$ , yields the desired goal.

With adversarial goals and capabilities defined, the final component of threat models pertains to *access*. Specifically, subsequent works have shown that adversaries need not have direct access to the victim model  $f$  to produce adversarial examples; models trained on similar data have similar decision manifolds, and thus, adversarial examples can “transfer” from one model to another [37, 38, 55]. When access is restricted (and thus, transferability is exploited), such threat models are called “grey-” or “black-box”, while full access to the victim model is called a “white-box” threat model. In this paper, we focus on white-box threat models as they represent the worst-case adversaries (in that they can produce adversarial examples with the tightest  $\ell_p$ -norm constraints). However, our decomposition and performance measurements can be directly applied to grey- and black-box threat models as well, which we further discuss in section 6.

**On  $\ell_p$ -norms.** As shown in Equation 1, the “cost” for crafting adversarial examples has been predominantly measured through  $\ell_p$ -norms. Informally, adversarial examples induce a misclassification between human and machine;  $\ell_p$ -bounded examples attempt to meet this definition. This concept arose from attacks on images, in that attacks would produce adversarial examples whose perturbations were invisible to humans, yet influential on models.  $\ell_p$ -norms are becoming an increasingly controversial topic, in that it has been debated if they have meaningful interpretations in non-visual domains [48], or even visual domains [10], or if they are useful at all [47]. Regardless, attacks have broadly converged on optimizing under  $\ell_0$ ,  $\ell_2$ , or  $\ell_\infty$ , and thus we focus our study on those.

### 2.2 Attack Algorithms

Here we briefly discuss the attack algorithms used in our decomposition (specifically, the unique components they introduce). We study these algorithms specifically due to their prevalence across works in adversarial machine learning [42].

**Basic Iterative Method (BIM).** BIM [29] is an iterative extension of Fast Gradient Sign Method (FGSM) [22]. BIM is an  $\ell_\infty$ -based attack that perturbs based on the gradient of a cost function, typically Cross-Entropy (CE). It often

uses Stochastic Gradient Descent (SGD) as its optimizer for finding adversarial examples.

**Projected Gradient Descent (PGD).** PGD [33] is widely regarded as the state-of-the-art in crafting algorithms. PGD is identical to BIM, with the exception of a *Random-Restart* preprocessing step, wherein inputs are initially randomly perturbed within an  $\ell_\infty$  ball.

**Jacobian-based Saliency Map Approach (JSMA).** The JSMA [39] is an  $\ell_0$ -based attack that is unique in its definition of a *saliency map*; a heuristic applied to the model Jacobian to determine the most salient feature to perturb in a given iteration. Unlike most other attacks, it does not rely on a cost function, but rather uses the model Jacobian directly. In our decomposition, we denote the JSMA saliency map as  $SM_J$ . The JSMA uses SGD as its optimizer.

**DeepFool (DF).** DF [35] is an  $\ell_2$ -based attack which models crafting adversarial examples as a projection onto the decision boundary. We find that we can model this projection as a saliency map, much like the JSMA, which we denote as  $SM_D$ . Similar to the JSMA, DF relies on the model Jacobian, does not have a cost function, and uses SGD.

**Carlini-Wagner Attack (CW).** CW [7] is an  $\ell_2$ -based attack that is unique across several dimensions: (1) it uses a custom loss, which we label Carlini-Wagner Loss (CWL), (2) introduces the *Change of Variables* technique, which ensures that, during crafting, the intermediate adversarial examples always comply with a set of box constraints, and (3) uses Adam as its optimizer for finding adversarial examples.

**AutoAttack (AA).** AA [15] is an ensemble attack consisting of three different white-box attacks (as well as one black-box attack). This ensemble is unique in that all of its attacks are parameter free (except for the number of iterations to run attacks for). Its white-box attacks are: (1) Auto Projected Gradient Descent - Cross Entropy (APGD-CE), which is PGD with the Momentum Best Start optimizer, (2) Auto Projected Gradient Descent - Difference of Logits Ratio (APGD-DLR), which is APGD-CE but with Difference of Logits Ratio Loss, and (3) Fast Adaptive Boundary Attack [13] (FAB), which is similar to DeepFool, but its optimizer Backward Stochastic Gradient Descent applies a biased gradient step and a backward step to stay close to the original point.

### 3 Decomposing AML

From analysis of popular attacks (discussed in subsection 2.2), we find that attacks broadly perform two main functions to produce adversarial examples, they: (1) manipulate  $x$ , such as with *Random-Restart*, or (2) manipulate gradients, such as by using a saliency map. We use this observation as a starting point for our decomposition; components that do the former are part of the *traveler* and ones that do the latter are within

Attack Algorithms																
Surface Components								Traveler Components								
Losses:								Random-Restart:								
Cross-Entropy								Enabled, Disabled								
Carlini-Wagner Loss																
Identity Loss																
Difference of Logits Ratio Loss																
Saliency Maps:								Change of Variables:								
$SM_J, SM_D, SM_I$								Enabled, Disabled								
$\ell_p$ -norm								Optimizer:								
$\ell_0, \ell_2, \ell_\infty$								SGD, Adam, MBS, BWSGD								
BIM	●	○	○	○	○	○	○	○	○	○	○	○	○	○	○	
PGD	●	○	○	○	○	○	○	○	○	○	○	○	○	○	○	
JSMA	○	○	●	○	○	○	○	○	○	○	○	○	○	○	○	
DF	○	○	○	○	○	○	○	○	○	○	○	○	○	○	○	
CW	○	○	○	○	○	○	○	○	○	○	○	○	○	○	○	
APGD-CE	○	○	○	○	○	○	○	○	○	○	○	○	○	○	○	
APGD-DLR	○	○	○	○	○	○	○	○	○	○	○	○	○	○	○	
FAB	○	○	○	○	○	○	○	○	○	○	○	○	○	○	○	
	CE	CWL	IL	DLR	SM <sub>J</sub>	SM <sub>D</sub>	SM <sub>I</sub>	ℓ <sub>0</sub>	ℓ <sub>2</sub>	ℓ <sub>∞</sub>	RR	CoV	SGD	Adam	MBS	BWSGD

Table 1: Attack Component Decomposition.

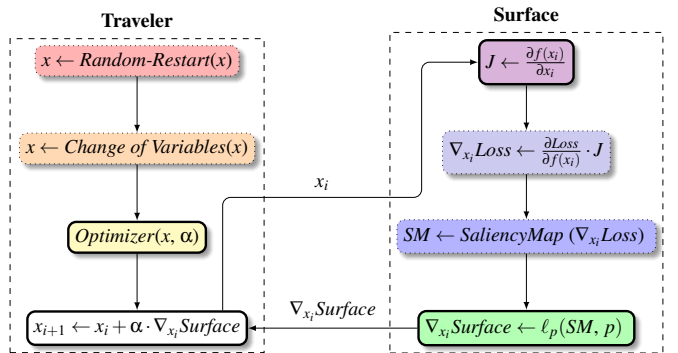


Figure 1: Flow of composition between the surface and traveler to construct an attack. Required components have bold outlines while optional components have dotted outlines.

the *surface*. Through this generalization, an attack can be seen as, simply, a choice of values for each of these components rather than a unique, incomparable entity.

Importantly, these components are broadly *mutually compatible* with one another, in that one could omit, add, or swap them when building an attack. We exploit this property when permuting components, therein yielding a vast space of attacks, some of which are known, but most of which are not. This modular view of attacks not only allows us to build this vast space, but also makes the framework highly extensible by nature; new attacks can add on new choices for components or even new components entirely. A summary of the evaluated components in this paper and the compositions of well-known attacks are shown in Table 1.

For the remainder of this section, we describe: (1) the components that constitute a surface and their options, (2) the layers that define a traveler and associated configurations, and (3) a characterization of the attack space. An overview of the composition of the surface and traveler, and their interaction is shown in Figure 1. All symbols defined in this section (and in the remainder of the paper) can be found in appendix D.

### 3.1 Surfaces

Surfaces, which encode the traversable attack space, are built from: (1) the model Jacobian, (2) the gradient of a loss function, (3) the application of a saliency map, and (4) an  $\ell_p$ -norm context of crafting adversarial examples.

**Model Jacobian.** At the heart of every surface (and thus, every attack) is the model Jacobian. The Jacobian  $\mathbf{J}$  of a model with respect to a sample  $x$  encodes the influence each feature  $i$  in  $x$  has over each class. While most attack papers encode perturbations as a function of the gradient of a loss function, such computations *necessarily* involve computing a portion (at least) of the model Jacobian (whether attacks require the full model Jacobian is a matter of design choice). This is evident via application of the chain rule:

$$\frac{\partial L(f(x), \hat{y})}{\partial x} = \frac{\partial L(f(x), \hat{y})}{\partial f(x)} \cdot \frac{\partial f(x)}{\partial x} = \frac{\partial L(f(x), \hat{y})}{\partial f(x)} \cdot \mathbf{J}$$

Importantly, computing a Jacobian is computationally expensive, on the order of  $O(d \cdot c)$ , where  $d$  describes the dimensionality of  $x$  (i.e., the number of features) and  $c$  describes the number of classes. Thus, attacks that *require* the full model Jacobian (e.g., JSMA and DF) must pay a (sometimes substantial) cost in compute resources to produce adversarial examples—a fact largely overlooked. This component is perhaps the one with the greatest potential for extensibility. For instance, black-box attacks or those wanting to overcome obfuscated gradients [2] could opt to use Backwards Pass Differentiable Approximation (BPDA) [2] to obtain a jacobian rather than a traditional backwards pass.

**Loss Functions.** Perhaps *the* most popular design choice in attack algorithms is to perturb features based on the gradient of a loss function. The intuition is straightforward: we rely on surrogate measurements to learn parameters that have maximal accuracy during training, and thus, we can exploit these same measures to produce samples that induce minimal accuracy. This is commonly Cross-Entropy (CE) loss:

$$\sum_i^c -\hat{y}_i \cdot \log(y_i)$$

where  $c$  is the number of classes,  $\hat{y}_i$  is the label as a one-hot encoded vector, and  $y_i$  is the output of the softmax function.

Aside from CE loss, other attack philosophies instead opt for custom loss functions that explicitly encode adversarial objectives, such as Carlini-Wagner Loss (CWL):

$$\|\delta\|_p^p + c \cdot \max(f_{\hat{y}}(x) - \max\{f_i(x) : i \neq \hat{y}\}, 0)$$

where  $p$  is the target  $\ell_p$ -norm to optimize under and  $c$  is a hyperparameter that controls the trade-off between the distortion introduced and misclassification.

Similar to the latter half of CWL, the Difference of Logits Ratio Loss (DLR) takes the difference between the true logit and the largest non-true-class logit. However, this

loss function also divides by the difference between the largest logit ( $f_{\pi_1}(x)$ ) and the third largest logit ( $f_{\pi_3}(x)$ ), as follows:

$$\frac{f_{\hat{y}}(x) - \max\{f_i(x) : i \neq \hat{y}\}}{f_{\pi_1}(x) - f_{\pi_3}(x)}$$

Finally, some attacks do not have an explicit loss function (such as JSMA or DF) and instead rely on information at other layers in the surface to produce adversarial examples (e.g., through saliency maps). To support this generalization, we implement a pseudo-identity loss function, Identity Loss (IL), which simply returns the  $\hat{y}$ th model logit component.

**Saliency Maps.** Saliency maps, in the context of adversarial machine learning, were first introduced by the JSMA [39]. These maps encode heuristics to best achieve adversarial goals by coalescing model Jacobian information into a gradient. We slightly tweak the original definition of the saliency map used in the JSMA to be: (1) independent of perturbation direction, and (2) agnostic of a target class. Though functionally different, we call this saliency map the Jacobian Saliency Map ( $SM_J$ ), as the underlying heuristic is identical in spirit to the one introduced by the JSMA:

$$SM_{J_i}(\hat{y}, \mathbf{J}) = \begin{cases} 0 & \text{if } \text{sgn}(J_{\hat{y},i}) = \text{sgn}(\sum_{j \neq \hat{y}} J_{j,i}) \\ |J_{\hat{y},i}| \cdot \sum_{j \neq \hat{y}} J_{j,i} & \text{otherwise} \end{cases}$$

where  $\hat{y}$  is the label for a sample  $x$ ,  $\mathbf{J}$  is the Jacobian of a model with respect to  $x$ , and  $i$  is the  $i$ th feature of  $x$ . Moreover, we observe that attack formulations with complex heuristics, such as DeepFool, can be cast as-is into a saliency map as well. We define the DeepFool Saliency Map ( $SM_D$ ) as:

$$SM_D(x, \hat{y}, q) = \frac{|f_{\hat{y}}(x) - f_k(x)|}{\|J_{\hat{y}} - J_k\|_q^q} \cdot (J_{\hat{y}} - J_k)^{q-1} \cdot \text{sgn}(J_{\hat{y}} - J_k)$$

where  $x$  is a sample,  $\hat{y}$  is the label for  $x$ ,  $q$  is calculated from the  $\ell_p$  norm where  $q = \frac{p}{p-1}$ ,  $f$  is the model, and  $k$  is the “closest” class to the true label  $\hat{y}$  calculated by:

$$k = \arg \min_{i \neq \hat{y}} \frac{|f_{\hat{y}}(x) - f_i(x)|}{\|J_{\hat{y}} - J_i\|_q}$$

Notably, unlike the  $SM_J$ , this formulation is identical to that presented in the original DeepFool attack.

Finally, attacks can also opt not to use any form of saliency map, and thus, we define an identity saliency map, Identity Saliency Map ( $SM_I$ ), which simply returns the passed-in gradient-like information as-is.

**$\ell_p$ -norms.** To meet threat model constraints, nearly all attacks manipulate gradient information via an  $\ell_p$ -norm. We remark that this can be conceptualized as a layer in a surface. Thus, we provide abstractions for three popular  $\ell_p$ -based threat models, defined as:

$$\ell_\infty(\nabla) = \text{sgn}(\nabla) \quad \ell_0(\nabla_i) = \begin{cases} \text{sgn}(\nabla_i) & \text{if } i = \arg \max(|\nabla|) \\ 0 & \text{otherwise} \end{cases}$$

$$\ell_2(\nabla) = \frac{\nabla}{\|\nabla\|_2}$$

where  $\nabla$  is some gradient-like information. While any  $\ell_p$ -norm could be used in this layer, we also see natural extensions to other measurements of distance, such as LPIPS [61] that could also fit into this component. This layer could also extend to allow for adaptive threat models, such what is used in the DDN attack [44].

### 3.2 Travelers

Travelers serve as the “vehicles” that navigate over a surface to meet adversarial goals. Travelers are built from a series of subroutines that modify  $x$ : (1) *Random-Restart*, (2) *Change of Variables*, and (3) an optimization algorithm. Here, we detail these components and describe how they aid in finding effective adversarial examples.

**Random-Restart.** Many optimization problems, such as  $k$ -means [24] and hill-climbing [45], have been shown to benefit from the meta-heuristic, *Random-Restart*. Due to non-linear activation functions, deep neural networks are non-convex, and thus, subject optimization algorithms to non-ideal phenomena. Specifically, *Random-Restart* attempts to prevent optimization algorithms from becoming stranded in local minima by applying a random perturbation to an input. At this time, PGD is unique in its use of *Random-Restart*, defined as:

$$x = x + \mathcal{U}(-\epsilon, \epsilon)$$

where  $\mathcal{U}$  is a uniform distribution, bounded by a hyperparameter  $\epsilon$  (which represents the total perturbation budget). Notably, while *Random-Restart* could be applied at each perturbation iteration, PGD uses it once on initialization.

**Change of Variables.** As a new way of enforcing box constraints, [7] introduced *Change of Variables* for the Carlini-Wagner Attack. As noted in [7], common practice for images is to first scale features to be within  $[0, 1]$ . When a perturbation is applied, these constraints must be enforced, as any feature beyond 1.0, for example, would map to a pixel value greater than 255, which exceeds the valid pixel range for 8 bit images. Most attacks enforce this constraint by simply clipping perturbations. However, this can negatively affect certain gradient descent approaches [7]. Thus, *Change of Variables* was proposed to alleviate deficient behaviors. In the context of CW, a variable  $w$  is defined and solved for (instead of the perturbation directly). Its relationship to  $x$  is:

$$x + \delta = \frac{1}{2}(\tanh(w) + 1)$$

where  $\delta$  is the resultant perturbation applied to an input  $x$ . As [7] notes, this ensures that  $0 \leq x + \delta \leq 1$ , meaning that examples will automatically fall within the valid input range.

**Optimizers.** Nearly all attacks are described as “taking steps in the direction” (of a cost function). Practically speaking, these attacks refer to Stochastic Gradient Descent (SGD). As demonstrated by the BIM, as little as three iterations (with  $\alpha = 0.01$ ) could be sufficient to drop state-of-the-art ImageNet models to  $\sim 2\%$  accuracy [29]. However,

Carlini-Wagner Attack was perhaps the first attack to explicitly use Adam to craft adversarial examples. Adam, unlike SGD, adapts learning rates for every parameter, and thus, often finds adversarial examples quicker than SGD [7].

In addition to SGD and Adam, we explore two additional optimizers, both of which come from AA. The first is Momentum Best Start (MBS), which accounts for momentum in its update step as follows:

$$x_{i+1} = x_i + \eta \cdot \alpha \cdot \delta_i + (1 - \eta) \cdot (x_i - x_{i-1})$$

where  $\eta$  controls the strength of the momentum (set to 0.75 in [15]). In addition to this momentum step, it also features an adaptive learning rate that updates based on conditions that capture progression of inputs toward adversarial goals, described in [15].

Finally, our framework also supports Backward Stochastic Gradient Descent (BWSGD), which is the optimizer used for FAB in [13]. This optimizer operates similarly to SGD and MBS but aims to update with the distance to the original sample in mind by updating as follows:

$$x_{i+1} = x_i + (1 - \eta) \cdot \alpha \cdot \delta_i + \eta \cdot (x_{org} + \alpha \cdot \delta_{org})$$

where  $\eta$  controls the influence of the original point on the update step. In addition, if  $x_i$  is misclassified, this optimizer also performs a backward step by moving  $x_i$  closer to  $x_{org}$  via:  $x_{i+1} = \beta \cdot x_{i+1} + (1 - \beta) \cdot x_{org}$ . In our experiments, we set  $\eta$  to be 0 since  $\delta_{org}$  (a) does not translate to attacks that do not use a decision hyperplane projection and (b) as can be seen in [13], the use of backward step had a far greater influence on the attack performance than setting a non-zero value of  $\eta$ .

## 4 Extending Performance Measurements

With the attack space made enumerable by our decomposition, we now focus on necessary extensions of budget interpretations, the introduction of Pareto Ensemble Attack, and our approach for measuring optimality.

### 4.1 Beyond the $\ell_p$ -norm

Since the inception of modern adversarial machine learning, the *cost* of producing an adversarial example has predominantly been measured through  $\ell_p$ -norms. Yet, it seems impractical to assume realistic adversaries will be unbounded by compute (as attacks that require days to produce adversarial examples offer little utility in any real-time environment). This observation is further exacerbated when attacks use expensive line search strategies [53], embed hyperparameter optimization as part of the crafting process [7], or rely on model Jacobian information [35, 39]. While such constructions can lead to incredibly effective attacks, adversaries who are limited by compute resources may find such attacks outright cost-prohibitive. To this end, we are motivated to extend standard definitions of budget beyond exclusive measurements of

$\ell_p$ -norms. Specifically, we incorporate and measure the *time* it takes to produce adversarial examples, therein extending our definition of budget as:

$$B(p, \theta, x) = \ell_p(x) + \theta \cdot T(x) \quad (2)$$

where  $p$  is the desired norm,  $\theta$  parameterizes the importance of computational cost versus the introduced distortion,  $x$  is the adversarial example, and  $T$  returns the compute time necessary to produce  $x$ . We note that the precise value of  $\theta$  depends on the threat model; adversaries who are compute-constrained may prioritize time twice as much as distortion (i.e.,  $\theta = 2$ ), while adversaries with strong compute may not consider time at all (i.e.,  $\theta = 0$ , as is done in standard evaluations). In [section 5](#), we find that some attacks consume prohibitively large amounts of budget when compute is measured, and thus, current threat models (which only measure  $\ell_p$  distance) fail to generalize adversarial capabilities.

## 4.2 Pareto Ensemble Attack

With a realistic interpretation of budgets, we revisit a fundamental question: *Does an optimal attack exist?* Attacks measure distortion through different  $\ell_p$ -norms, can require different amounts of compute, and have varying budgets (which is notably true for robustness evaluations). Thus, answering this question is non-trivial, especially in the absence of any meaningfully large attack space.

A single definition that accurately characterizes optimality across attacks, while incorporating these confounding factors, is challenging. Yet, we can say some attack  $A$  is *optimal* if, for a given threat model,  $A$  bounds all other attacks for an adversarial goal (i.e.,  $A$  must lower-bound all attacks when minimizing model accuracy across budgets). Of the 576 attacks that we evaluated, no single attack met this definition. Thus, we conclude that the optimal attack are best characterized by an *ensemble of attacks*.

To this end, we introduce the Pareto Ensemble Attack (PEA), a theoretical attack which, for a given budget and adversarial goal, returns the set of adversarial examples that best meet the adversarial goal, within the specified budget (in other words, the Pareto frontier). The PEA is attractive for our analysis, in that it serves as a meaningful baseline from which we can compare attack performance to (discussed in the following section). Moreover, as an ensemble, the PEA naturally evolves as the evaluated attack space expands. We formally define the PEA as:

$$\text{PEA} = \bigcup_{b \in \mathcal{B}} \left\{ \arg \min_{x_A \in \mathcal{A}} \text{Acc}(f(x_A), \hat{y}) \mid B(p, \theta, x_A) \leq b \right\}$$

where  $b$  is a budget in a list of budgets  $\mathcal{B}$ ,  $x_A$  is the set of adversarial examples produced by attack  $A$  from a space of attacks  $\mathcal{A}$ ,  $f$  is a model,  $\hat{y}$  is the set of true labels for  $x_A$ ,  $B$  is a function used to measure budget (i.e., [Equation 2](#)),  $\text{Acc}$  returns

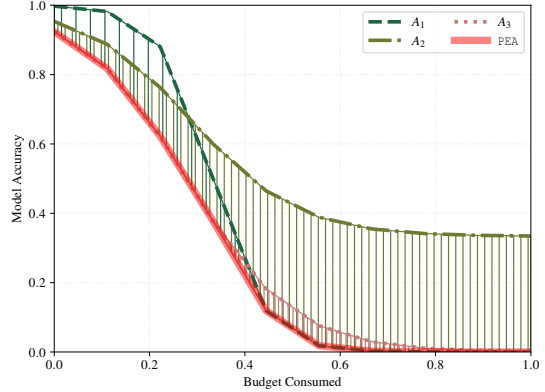


Figure 2: The Optimal Attack — The PEA lower-bounds all attacks across the range of budgets. Attacks  $A_1$  and  $A_3$  define the PEA for different budget ranges, while  $A_2$  is never part of the PEA. The area between the PEA and attack curves are shown with vertical bars.

model accuracy,  $p$  is an  $\ell_p$ -norm, and  $\theta$  controls the sensitivity to computational resources. Concisely, the PEA returns the set of adversarial examples whose model accuracy is minimal and within budget. Moreover, we provide a visualization of the PEA in [Figure 2](#), where the PEA forms the *lower envelope* of model accuracy across budgets. We highlight that if there was some attack  $A'$  which achieved the lowest accuracy across all budgets (for some domain), then the PEA =  $A'$ . It has been suggested by some in the community that algorithms such as PGD might be optimal for some application [\[5, 33, 62\]](#). Our formulation of the PEA and measure of optimality allows us to test this hypothesis.

**Measuring Optimality.** The PEA yields a baseline from which we can fairly assess the performance of attacks. As the PEA meets the definition of *optimal* (that is, it bounds attack performance), we can evaluate attack performance relative to the PEA. Intuitively, attacks that closely track the PEA are performant, while those that do not are suboptimal. Mathematically, this can be measured as the area between the curves of the PEA and some attack  $A$ . We note that our definition of optimality is: (1) relative to the attacks considered (and not measured against a set of provably worst-case adversarial examples or certified robustness [\[5, 43, 57\]](#)), and (2) as attacks are ranked by area, prefers attacks that are consistently performant (i.e., across the budget space). We acknowledge this measurement favors attacks whose behaviors are stable (which we argue most popular white-box attacks exhibit); other modalities may benefit from other cost measures.

For example, in [Figure 2](#), the area between the PEA and attack  $A_2$  is maximal, minimal for attack  $A_3$ , and somewhere in between for attack  $A_1$ . Thus, we conclude that the worst-case adversary would use  $A_3$  if bound by small budgets, otherwise  $A_1$  (and never  $A_2$ ). This approach to measuring attack per-

formance is desirable in that, (1) attacks that track the PEA across budgets have minimal area (and thus, constitute a performant attack), and (2) attacks that are exclusively optimal for specific budgets incur large area, which allows us to differentiate attacks that are *always* performant from those that are *sometimes* performant.

## 5 Evaluation

With our attack decomposition and approach to measure optimality, we ask several questions: (1) Do known attacks perform best? (2) What attacks are optimal, if any? (3) Which components tend to yield performant attacks?

### 5.1 Setup

We perform our experiments on a Tensor EX-TS2 with two EPYC 7402 CPUs, 1 TiB of memory, and four Nvidia A100 GPUs. We use PyTorch [40] 1.9.1 for instantiating learning models and our attack decomposition. Here, we describe the attacks, threat models, robustness approach (i.e., adversarial training), and datasets used in our evaluation. We defer attack adaptations to [appendix D.1](#), and hyperparameters & details on adversarial training to [appendix D](#).

**Attacks.** In [section 3](#), we introduce a decomposition of adversarial machine learning by atomizing attacks into modular components. Our evaluation spans the enumerated 576 attacks. Of these 576, JSMA, CW, DF, PGD, BIM, APGD-CE, APGD-DLR, and FAB are labeled explicitly, while other attacks are numbered from 0 to 575. The specific component choices of attacks mentioned by number can be found in [appendix A](#). We note that some known attacks (such as DF and CW) have specialized variants for  $\ell_{p \neq 2}$ -norms, which we do not implement (as to maintain homogeneous behaviors across attacks of the same norm). Thus, we still reference these attacks numerically, since they are not the algorithmically identical.

In our experiments, we focused on untargeted attacks: that is, the adversarial goal is to minimize accuracy. While our decomposition is readily amenable to targeted variants, we defer analysis (and thus evaluation) of targeted attacks for two reasons: (1) choosing a target class requires domain-specific justification, and (2) certain classes are harder to attack than others [39]. These two factors would require a rather nuanced analysis, while our objectives aim to characterize broad attack behaviors. Thus, we anticipate that while a targeted analysis might affect attack performance in an absolute sense, relative performance to other attacks will likely be indifferent.

**Threat Models.** As motivated in [section 4](#), we explore the interplay in attack performance when compute is measured, as defined by [Equation 2](#). Specifically, we explore 3  $\ell_p$ -based threat models (i.e.,  $\ell_0$ ,  $\ell_2$ , and  $\ell_\infty$ ) with 20 different values of  $\theta$  at 0.1 step sizes, from 0 to 2. These values can be interpreted as an adversary who, for example, values computational speed

*twice as much* over minimizing distortion (i.e.,  $\theta = 2$ ). We note that all attacks are instantiated within our framework, and thus, any implementation-specific optimizations that accelerate compute speed are leveraged uniformly across attacks.

**Robust Models.** Adversarial training [22, 33] is one of the most effective defenses against adversarial examples to date [5, 14, 46]. Given its popularity and compelling results, we are motivated to investigate the impact of robust models on relative attack performance. We adversarially train our models with a PGD-based adversary. We follow the same approach as shown in [33]: input batches are replaced by adversarial examples (produced by PGD) during training. For MNIST and CIFAR-10, hyperparameters were used from [33]; other datasets were trained with parameters which maximized the accuracy over benign inputs and adversarial examples. Additional hyperparameters can be found in [appendix D](#).

#### 5.1.1 Datasets

We use seven different datasets in our experiments, chosen for their variation across dimensionality, sample size, and phenomena. We provide details and basic statistics below.

**Phishing.** The Phishing [12] dataset is designed for detecting phishing websites. Features were extracted from 5000 phishing websites and 5000 legitimate webpages. It contains 48 features and 10 000 samples. Beyond its phenomenon, we use the Phishing dataset to investigate the effects of small dimensionality and training size on attack performance.

**NSL-KDD.** The NSL-KDD [54] is based on the seminal KDD Cup '99 network intrusion detection dataset. Features are defined from varying network features from traffic flows emulated in a realistic military network. At 41 features, it contains 125 973 samples for training and 22 544 for testing. We use the NSL-KDD for its small dimensionality, large training size, and concept drift [21].

**UNSW-NB15.** The UNSW-NB15 [36] is a network intrusion detection dataset designed to replace the NSL-KDD. Features are derived from statistical and packet analysis of real innocuous flows and synthetic attacks. It has 48 features, with 175 341 samples for training and 83 332 samples for testing. The UNSW-NB15 enables us to compare if attacks generalize to similar phenomenon (such as the NSL-KDD).

**MalMem.** CIC-MalMem-2022 (MalMem) [8] is a modern malware detection dataset. 58 features are extracted from memory dumps of benign applications and three different malware families (i.e., trojans, spyware, and ransomware). In total, it contains 58.596 samples, with half belonging to benign applications and half to malware. MalMem gives us the opportunity to understand the effects of small dimensionality in an entirely different phenomenon from the network datasets.

**MNIST.** MNIST [30] is a dataset for handwritten digit recognition. It is a well-established benchmark in adversarial machine learning applications. With 784 features, 60 000 samples for

training and 10 000 for testing, MNIST has substantially larger dimensionality than even the largest network datasets. We use MNIST to corroborate prior results, explore a vastly different phenomenon, and investigate how (relatively) large dimensionality influences attack performance.

**FMNIST.** Fashion-MNIST (FMNIST) [58] is a dataset for recognizing articles of clothing from Zalando articles. Advertised as a drop-in replacement for MNIST, FMNIST was designed to be a harder task and closer representative of modern computer vision challenges. FMNIST has identical dimensionality, training samples, and test samples to MNIST. Thus, we use FMNIST to understand if changes in phenomena alone are sufficient to influence attack performance.

**CIFAR-10.** CIFAR-10 [28] is a dataset for object recognition. Like MNIST, CIFAR-10 is extensively used in adversarial machine learning literature. At 3072 features, CIFAR-10 represents a substantial increase in dimensionality from MNIST. It has 60 000 samples for training and 10 000 for testing. CIFAR-10 allows us to compare against extant works and explore how domains with extremely large dimensionality affect attack efficacy.

## 5.2 Comparison to Known Attacks

As discussed in section 3, we contribute 568 new attacks. Naturally following, we ask: *are any of these attacks useful?* Asked alternatively, *do known attacks perform best?* We investigate this question through commonly accepted performance measurements [6, 29, 35, 39]: the amount of  $\ell_p$  budget consumed by attacks whose resultant adversarial examples cause model accuracy to be  $<1\%$ . In this traditional performance setting, we aim to understand if known attacks serve as the Pareto frontier (which would indicate that our contributed attacks yield little in terms of adversarial capabilities).

We organize our analysis as follows: (1) we first segment attacks based on  $\ell_p$ -norm and compare them to known attacks of the same norm (that is, we compare JSMA to  $\ell_0$  attacks, CW, DF, & FAB to  $\ell_2$ , and PGD, BIM, APGD-CE, & APGD-DLR to  $\ell_\infty$ ), and (2) report relative budget consumed (with respect to known attacks) for attacks whose adversarial examples caused model accuracy to be  $<1\%$ .

### 5.2.1 Performance on MNIST

For our analysis of attack performance, we craft adversarial examples for 1000 iterations over ten trials (we note that 1000 iterations was selected for completeness; the vast majority of attacks converged in less than 100 iterations). Figure 3 shows the median results for two threat models, segmented by  $\ell_p$ -norm. Known attacks (i.e., JSMA, CW, DF FAB, PGD, BIM, APGD-CE, and APGD-DLR) are highlighted in red, while other attack curves are dotted blue and slightly opaque to capture density. We now discuss our results on a per-norm basis.

**$\ell_0$  Attacks.** Figure 3a shows  $\ell_0$ -targeted attack performance with the JSMA in red. We observe that the JSMA is worse than most attacks. Attack performance is largely well-clustered with a few poor performing attacks near the top right portions of the graph. These attacks used *Random-Restart*, and thus, immediately consume most of the available  $\ell_0$  budget.

**$\ell_2$  Attacks.** Figure 3b shows  $\ell_2$ -targeted attacks, with CW as solid red, DF as dash-dotted red, and FAB as dashed red. Like  $\ell_0$ , attacks are well-concentrated (albeit with slightly more spread). Notably, DF and FAB (which are ostensibly superimposed on one another), demonstrate impressive performance (the red lines that are nearly vertical)—both drop model accuracy with a near-zero increase in budget. CW exhibits moderate performance over the budget space.

**$\ell_\infty$  Attacks.** Figure 3c shows  $\ell_\infty$ -targeted attacks, with PGD as solid red, BIM as dash-dotted red, APGD-CE as dashed red, and APGD-DLR as dotted red. Unlike other norms,  $\ell_\infty$  has clear separation, broadly attributable to using *Change of Variables* (specifically, attacks that used *Change of Variables* performed worse than those that did not). Finally, all of the known attacks exhibit near-identical performance, with APGD-DLR slightly pulling ahead at budgets  $> 0.2$ .

From our norm-based analysis, we highlight that: (1) *Random-Restart* is largely inappropriate for  $\ell_0$ -targeted attacks (in that benefits do not outweigh the cost), (2)  $\ell_2$ -targeted attacks cluster fairly well; no individual attack substantially outperformed any other, and (3)  $\ell_\infty$ -targeted attacks were broadly unable to exploit *Change of Variables*.

### 5.2.2 Relative Performance to Known Attacks

Recall our central question for this experiment: *do known attacks perform best?* To answer this question, we analyze the minimum budget necessary for attacks to cause model accuracy to be  $<1\%$  (attacks that fail to do so are encoded as consuming infinite budget). We run attacks for 1000 iterations over ten trials and report the median results in Table 2. Here, attacks are ranked by budget and segmented by norm (i.e., 192 attacks per norm). We report the percentage change of each attack with respect to the known attack that performed best in that norm (that is, for  $\ell_0$ , results are relative to the JSMA, while for  $\ell_2$ , results are relative to CW, which outperformed DF, etc.). In the table, we show: (1) the attack that ranked first, (2) ranks of known attacks, and (3) the lowest ranked attack that still reduced model accuracy to  $<1\%$ . Next, we highlight some strong trends for each  $\ell_p$ -norm.

Of the 34% of attacks that succeed in the  $\ell_0$  space, the JSMA (ranked 32<sup>nd</sup>) was at the bottom of the highly performant bin (in that its  $\ell_0$  budget was 0.17)—the JSMA was held back by its saliency map,  $SM_J$ ; using either  $SM_D$  (or no saliency map at all, i.e.,  $SM_T$ ) was almost always better. While CW seemingly rank low (i.e., 69<sup>th</sup>), we note that  $\ell_2$  budgets were broadly similar, as the worst and best performing attacks were within  $\pm 50\%$  of the budget consumed by CW. APGD-DLR,



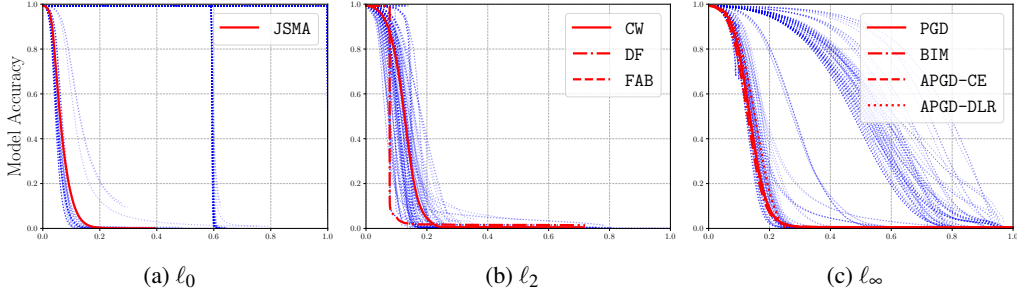


Figure 3: MNIST model accuracy for (normalized)  $l_0$ -,  $l_2$ -, and  $l_\infty$ -based budgets. Known attacks are highlighted in red. Results show median accuracy across 1000 iterations over 10 trials.

$l_0$ Attacks				$l_2$ Attacks				$l_\infty$ Attacks			
Rank	Attack	% Reduction	$l_0$ Budget	Rank	Attack	% Reduction	$l_2$ Budget	Rank	Attack	% Reduction	$l_\infty$ Budget
1.	ATK <sub>171</sub>	-41 %	0.10	1.	ATK <sub>460</sub>	-50 %	0.12	1.	ATK <sub>449</sub>	-8 %	0.22
30.	<b>JSMA</b>	—	0.17	69.	<b>CW</b>	—	0.24	17.	<b>APGD-DLR</b>	—	0.24
68.	ATK <sub>246</sub>	+352 %	0.77	88.	ATK <sub>37</sub>	+45 %	0.35	40.	<b>BIM</b>	+16 %	0.28
				136.	<b>DF</b>	+∞%	∞	48.	<b>APGD-CE</b>	+20 %	0.29
				137.	<b>FAB</b>	+∞%	∞	49.	<b>PGD</b>	+20 %	0.29
								135.	ATK <sub>191</sub>	+304 %	0.97

Table 2: MNIST Relative Attack Comparisons. Budgets are normalized. Attacks that fail to reduce model accuracy to be  $<1\%$  are labeled as consuming infinite budget. Budget reductions are relative to the best known attack for each  $l_p$ -norm.

BIM, APGD-CE, and PGD, ranked 17<sup>th</sup>, 40<sup>th</sup>, 48<sup>th</sup>, and 49<sup>th</sup> respectively, were marginally outperformed by attacks using either the  $SM_D$  saliency map or BWSGD optimizer. As a final note, we were confounded by the performance of DF and FAB—visually inspecting Figure 3b, both are clearly superior attacks (the performance curves ostensibly resemble square waves) and yet, they failed to reduce model accuracy to  $<1\%$ . While these analyses of attack performance has been useful historically for understanding adversarial examples, we argue that this “race to 0% accuracy” fails to capture meaningful definitions of attack performance (as made evident by the apparent “failure” of DF and FAB).

From our comparison with known attacks, we highlight two key takeaways: (1) Measuring the required distortion to reach some amount of model accuracy is a rather crude approach to estimating attack performance. We argue using measurements that factor the entire budget space (such as the PEA, which we use subsequently) will yield more meaningful interpretations of attack performance. (2) Even when we define success as  $<1\%$  model accuracy, known attacks do not perform best. In fact, many attacks produced by our decomposition consistently outperformed known attacks (e.g., 68 out of the 189 introduced by our approach outperformed both CW and DF), which demonstrates the novel adversarial capabilities introduced by our decomposition.

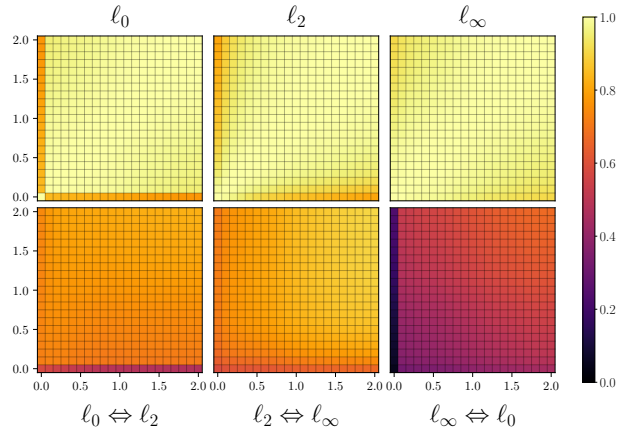


Figure 4: Median Spearman Rank Correlation Coefficients for MNIST—Results are segmented by  $l_p$ -norm. Data points correspond to a specific threat model (i.e., a value for  $\theta$ ). High attack performance generalization is encoded as lighter shades, while low generalization is encoded with darker shades. Top row shows within-norm generalization & bottom row shows cross-norm generalization.

### 5.3 Optimal Attacks

In Figure 4.2, we introduced an approach for measuring optimality: the area between the performance curves of the PEA and an attack. Attacks that have a small area closely track the PEA and thus, are performant attacks, while those that have a

large area perform poorly. In this experiment, we ask: *does attack performance generalize?* In other words, is relative attack performance invariant to dataset or threat model?

We investigate this hypothesis of attack optimality by ranking attacks by area across varying threat models, datasets, and robust models. Then, we measure the generalization of these rankings via the Spearman rank correlation coefficient [51], which informs us how similar the rankings are between two datasets, threat models, or a robust and non-robust model.

For example, a highly positive correlation across two datasets would imply that relative attack performance was unchanged (in other words, changing the dataset had little to no effect on attack performance), a near-zero correlation would suggest that relative attack performance changed substantially (which would suggest attack performance is sensitive to the dataset), and a negative correlation would indicate attack performance was reversed (i.e., the worst attacks on one dataset became the best on another). In our experiments, we craft adversarial examples for 1000 iterations over ten trials<sup>1</sup> and report the median Spearman rank correlation coefficients. We note that 1000 iterations was selected for completeness; the vast majority of attacks converged in less than 100 iterations.

**Optimal Attacks by Threat Model.** Here, we analyze the generalization of attack performance *across threat models*. Specifically, we consider  $\ell_0$ -,  $\ell_2$ -, and  $\ell_\infty$ -based threat models with varying values of  $\theta$  (from 0 to 2). Note that  $\theta = 0$  (i.e., where compute time is ignored) is the commonly used threat model. Figure 4 shows the median Spearman rank correlation coefficients for MNIST (other datasets are listed in appendix C) with results segmented by  $\ell_p$ -norm. Each entry corresponds to a unique threat model (i.e., a value for  $\theta$ ). High attack performance generalization is encoded as lighter shades, while low generalization is encoded with darker shades.

From the results, we can readily observe: (1) rankings do not generalize across  $\ell_p$ -norms, especially between  $\ell_0$ - and  $\ell_\infty$ -targeted attacks (but do generalize relatively well *within* an  $\ell_p$ -norm), and (2) the influence of compute on rankings appears to be  $\ell_p$ -norm dependent:  $\ell_0$ -based threat models that weight compute (i.e.,  $\theta \neq 0$ ) do not generalize well to those that do not,  $\ell_2$ -based threat models exhibit a smoother degradation of generalization, while, surprisingly,  $\ell_\infty$ -based threat models generalize *everywhere* (that is, the same attacks that were found to be performant with  $\theta = 2$  were as performant when  $\theta = 0$ ). Within a dataset, we observe that the threat model significantly affects attack performance across  $\ell_p$ -norms, and to some extent, within an  $\ell_p$ -norm, with  $\ell_\infty$  as the exception.

**Optimal Attacks by Dataset.** In this experiment, we instead now measure the generalization of attack performance *across datasets*. Specifically, for a given threat model, we measure the generalization of attack performance rankings

across seven datasets. The evaluated datasets span varying forms of phenomena, from classifying network traffic to categorizing clothing items, and thus, we investigate if performant attacks are task-agnostic. Correlations for threat models with  $0 < \theta < 2$  can be found in appendix C.

The results in Figure 5 disclose that: (1) CIFAR-10 does not generalize at all, regardless of  $\ell_p$ -norm, (2) skewing budgets towards favoring compute gradually degrades generalization—attack rankings become increasingly dissimilar as we move from ignoring compute time ( $\theta = 0$ ) to heavily favoring it ( $\theta = 2$ ), and (3)  $\ell_0$ -based threat models readily generalize across datasets and is largely invariant to considering compute,  $\ell_2$  attacks, regardless of  $\theta$ , moderately generalize, and  $\ell_\infty$  attacks closely track  $\ell_2$  attacks with a particular subtlety: attacks performant on MNIST generalized almost perfectly to FMNIST (i.e., image-based generalization), while attacks performant on NSL-KDD almost perfectly generalized to UNSW-NB15 (i.e., network-intrusion-detection-based generalization). Lastly, we observe that attacks performant on Phishing and MalMem moderately generalized better to non-image data (particularly to the UNSW-NB15). Considering compute degrades these observations slightly. Within a threat model, we observe that, based on  $\ell_p$ -norm, the dataset can have drastic degrees of influence on attack performance, in that it can have little effect at all (e.g.,  $\ell_0$ ), have an effect everywhere (i.e.,  $\ell_2$ ), or have an effect specific to the phenomena (i.e.,  $\ell_\infty$ ). We attribute the unique behavior of CIFAR-10 to its dimensionality; the next largest dataset, FMNIST and MNIST, are  $\sim 74\%$  smaller.

**Optimal Attacks Against Robust Models.** In this final experiment, we now measure the generalization of attack performance *between robust and non-robust models*. Specifically, for a given threat model and dataset, we compute pairwise correlations between attack performance rankings on robust and non-robust models. Adversarially trained models have been shown to be an effective defense against adversarial examples [33], and thus, we investigate if such procedures have a visible effect on attack performance.

Median Spearman rank correlation coefficients for all datasets and threat models are shown in Figure 6. We note several trends across norm, threat models, and datasets: (1) generally speaking, attack rankings in  $\ell_2$ -based threat models were *substantially* affected by robust models, especially for MalMem, MNIST, and FMNIST, (2) considering compute can have a significant impact on generalization, mainly dependant on the norm; increasing the importance of compute almost universally aided generalization in  $\ell_2$ , but hurt generalization in  $\ell_0$  (especially for image data, albeit CIFAR-10 is less sensitive to varying  $\theta$  at the scales we investigated), and (3) we observed that top-performing attacks can be especially affected: on MNIST for an  $\ell_2 + 0 \cdot$  time threat model, for instance, the top 10 attacks on the non-robust model had a median rank of 445<sup>th</sup> (out of 576) on the robust model. These profound differences in relative attack effectiveness demonstrate that

<sup>1</sup>In another experiment, we validated that rankings are highly correlated across trials. Combined with our use of nonparametric statistics (i.e., median Spearman correlation), this ensures our metrics converge in few trials.

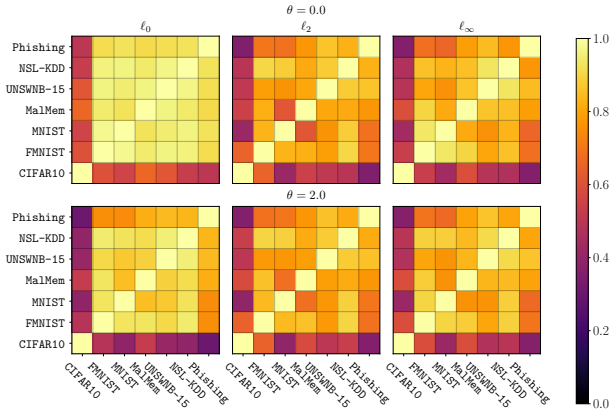


Figure 5: Median Spearman Rank Correlation Coefficients for  $\theta = 0$  and  $\theta = 2$  threat models—Results are segmented by  $\ell_p$ -norm. Entries correspond to a dataset pair. High attack performance generalization is encoded as lighter shades, while low generalization is encoded with darker shades.

the unique properties of robust models necessitate changes to attack components (discussed further in [subsection 5.4.3](#)).

**Takeaways on Attack Optimality.** In this set of experiments, we analyzed attack optimality through the lens of varying threat models, unique data phenomena, and robust models. From our analyses, we find that the optimality of any given attack is highly dependant on the given context. We support this conclusion through the following remarks on the generalization of relative attack performance: (1) across threat models, performance generalizes well within an  $\ell_p$ -norm, but not across—considering compute exacerbates this observation, (2) across datasets, performance generalization is broadly sensitive to  $\ell_p$ -norm (with CIFAR-10 generalizing poorly everywhere), and (3) between robust and non-robust models, attack rankings are largely a function of data phenomena (e.g., image-based phenomena exhibit poor generalization, regardless of the threat model).

## 5.4 When and Why Attacks Perform Well

With our metric for attack performance established and evaluated, we proceed by asking, *why do certain attacks perform well?* Here, we explore the general trends of attack components and their influence on performance through a series of hypothesis tests. We build a space of possible hypotheses of relative attack performance (over all attack components), perform hypothesis testing against this space, and identify those with the highest significance and effect size. We begin with significant hypotheses of non-robust models and conclude with hypotheses most affected by model robustness.

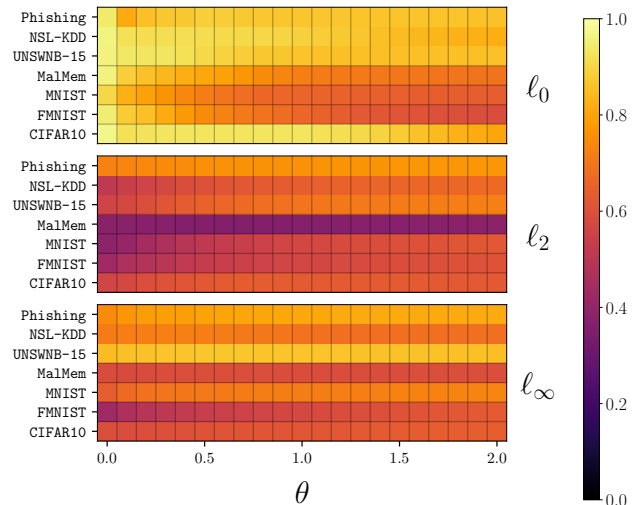


Figure 6: Median Spearman Rank Correlation Coefficients for robust and non-robust models—Results are segmented by  $\ell_p$ -norm. Data points correspond to a specific threat model (i.e., a value for  $\theta$ ). Lighter shades show high generalization of attack performance ranking across that dataset and threat model, while darker shades are low generalization.

### 5.4.1 The Space of Hypotheses

We define a *hypothesis* as a comparison between two component values (which we label as  $H_1$  and  $H_2$ ), such as “*using Cross-Entropy is better than Carlini-Wagner Loss.*” Now, we want to understand the *conditions* that make a hypothesis true. These conditions can be using a specific dataset, under a certain threat model, or based on other component values. Building off our previous example, this hypothesis paired with a condition could be “*using Cross-Entropy is better than Carlini-Wagner Loss, when the dataset is Phishing.*” When we test a hypothesis, we look at the statistical significance of the hypothesis under all conditions to determine when a hypothesis is true. Enumerating across all possible hypothesis and condition pairs yielded 1690 candidate hypotheses. It should be noted that the component values in hypotheses are always in the same component, as comparing usefulness across components would be nonsensical (e.g., “Using Cross-Entropy is better than using *Random-Restart*” is not meaningful).

### 5.4.2 Testing

We test the 1690 hypotheses with the Wilcoxon Signed-Rank Test, a non-parametric pairwise test, equivalent to a pairwise Mann-Whitney  $U$  Test, to determine its significance. We also report the effect size of the test, defined as the percentage of pairwise median areas (over ten trials, with trial counts factored into computed  $p$ -values) from component  $H_1$  that were smaller than component  $H_2$  (recall, a smaller area corresponds

	Component H <sub>1</sub>		Component H <sub>2</sub>		Condition	p-value	Effect Size
1.	SGD	is better than	BWSGD	when	Dataset = MNIST	$<2.2 \times 10^{-308}$	99 %
2.	Adam	is better than	BWSGD	when	Dataset = MNIST	$<2.2 \times 10^{-308}$	99 %
		⋮					
84.	Identity Loss	is better than	Difference of Logits Ratio Loss	when	Dataset = NSL-KDD	$<2.2 \times 10^{-308}$	93 %
85.	SGD	is better than	BWSGD	when	SaliencyMap = Jacobian Saliency Map	$<2.2 \times 10^{-308}$	92 %
		⋮					
393.	DeepFool Saliency Map	is better than	Jacobian Saliency Map	when	Dataset = FMNIST	$<5 \times 10^{-6}$	66 %
394.	Cross-Entropy	is better than	Carlini-Wagner Loss	when	Change of Variables = Disabled	$<5 \times 10^{-6}$	61 %
		⋮					
1689.	$\ell_0$	is better than	$\ell_2$	when	Threat Model = $\ell_2 + 1.0$	$9.8 \times 10^{-1}$	50 %
1690.	Identity Saliency Map	is better than	DeepFool Saliency Map	when	Threat Model = $\ell_\infty + 0.4$	1.0	49 %

Table 3: The evaluated hypotheses for non-robust models. The top 344 hypotheses have a  $p$ -value that exhibits 64 bit underflow. When sorted by effect size, the top 50 % of hypotheses have an effect size greater than 80 %.

to a better attack, as it more closely tracks the PEA). Note that the  $p$ -values for many hypotheses underflowed 64 bit floating point precision, implying that the results of the test are highly significant across all datasets and threat models. A subset of of hypotheses are represented in Table 3.

We find many highly-significant correlations in the results across the space of hypotheses. Specifically, we set a significance threshold proportional to the number of hypothesis tests we evaluated to minimize false positives<sup>2</sup>:  $p < \frac{0.01}{1690} = 5 \times 10^{-6}$ . We found that 1536 (90 %) of hypotheses were below this threshold. We highlight the most prominent conclusions among these 1536 hypothesis: **(1)** *Change of Variables* was found to be disadvantageous—86 hypotheses involving *Change of Variables* met our threshold; all 86 were against its use, **(2)** Adam was superior to all other optimizers—503 hypotheses comparing Adam to other optimizers met our threshold, of which 50 % of them ruled in favor of Adam (with SGD at 33 %, and MBS at 16 %), **(3)** *Random-Restart* was found to be preferable across 61 % of hypotheses (51 of 83), **(4)**  $\ell_\infty$ -targeted attacks, at 79 % (163 of 205) were superior to both  $\ell_0$ - and  $\ell_2$ -targeted (which were only favorable 16 % (34 of 205) and 4 % (8 of 205) of the time, respectively), **(5)** using no saliency map (i.e.,  $SM_\perp$ ) was better 70 % (131 of 187) of the time, **(6)** perhaps surprisingly, using no loss function was more advantageous 47 % (224 of 472) of the time, over CE and CWL, which were useful 34 % (161 of 472) and 18 % (87 of 472) of the time, respectively, and **(7)** contrary to common practice, using  $\ell_\infty$ -based attacks were sometimes superior to  $\ell_2$ -based attacks for  $\ell_2$ -based threat models (21 of 42); this result would suggest that perturbing based on the magnitude of gradients, while effective, can be excessive (when measuring cost under  $\ell_2$ ) and unnecessary to meet adversarial goals.

We highlight some key takeaways from this experiment: (1) These hypothesis tests provide statistical evidence of some common practices within the community (using *Random-Restart* and the superiority of Adam), while also demonstrating some perhaps surprising conclusions, such as the detriment of using *Cross-Entropy* over no loss function at all. (2) We

<sup>2</sup>One would expect evaluating 1000 hypotheses at  $p < 0.01$  significance would result in 10 false positives, for example.

emphasize the utility of hypothesis testing for threat modeling as well: the tests provide a schema for performing worst-case benchmarks in their respective domain. For example, when benchmarking MNIST against  $\ell_0$ -based adversaries, attacks that use the Jacobian Saliency Map are likely to outperform attacks that use DeepFool Saliency Map.

### 5.4.3 The Effect of Model Robustness

As shown in Figure 6, robust models can have a significant impact on attack rankings. Here, we investigate why such broad phenomena occur. Specifically, we investigate how attack parameter choices change performance on a robust versus a non-robust model. We repeat our hypothesis testing on robust models only and compare the hypotheses most affected (that is, the largest changes in effect size) by robust models.

Table 4 provides a listing of the top pairs of hypotheses, sorted by the change in effect size from a non-robust to robust model (labeled as delta). Many of the top hypotheses when migrating from non-robust to robust models largely concern CIFAR-10 and MalMem, which were broadly the most unique phenomena across our experiments. Specifically, we see large changes in losses and saliency maps for the attacks that were effective at attacking robust models. The emphasis on CE could be in part attributed to the fact that both the model is trained on this loss as well as used by PGD, the attack used to generate adversarial examples within minibatches. This observation suggests that alignment between between attack losses and losses used for adversarial training is highly effective at attacking robust models.

Beyond the influence of loss on CIFAR-10 and MalMem, most of our tested hypotheses remained relatively unaffected by model robustness: of the 1690 hypotheses tested, only 334 had an effect size change of 10 % or greater between robust and non-robust models. This implies that, while many of the factors that make attacks effective do not vary between normally- and adversarially-trained models, the subset that *does* vary accounts for a vast difference in attack effectiveness.

	Component H <sub>1</sub>		Component H <sub>2</sub>		Condition	p-value	Effect Size	Delta
1.	Cross-Entropy	is better than	Difference of Logits Ratio Loss	when	Dataset = CIFAR-10	$<2.2 \times 10^{-308}$	96 %	45 %
2.	Identity Saliency Map	is better than	DeepFool Saliency Map	when	Dataset = CIFAR-10	$<2.2 \times 10^{-308}$	74 %	44 %
3.	Difference of Logits Ratio Loss	is better than	Carlini-Wagner Loss	when	Dataset = NSL-KDD	$<1 \times 10^{-5}$	57 %	44 %
4.	Cross-Entropy	is better than	Identity Loss	when	Dataset = MalMem	$<2.2 \times 10^{-308}$	69 %	43 %
5.	<i>Random-Restart: Disabled</i>	is better than	<i>Random-Restart: Enabled</i>	when	Optimizer = BWSGD	$<2.2 \times 10^{-308}$	92 %	41 %
6.	Adam	is better than	SGD	when	Dataset = MalMem	$<1 \times 10^{-5}$	46 %	39 %
7.	<i>Random-Restart: Disabled</i>	is better than	<i>Random-Restart: Enabled</i>	when	Dataset = MalMem	$<2.2 \times 10^{-308}$	90 %	35 %
8.	Identity Loss	is better than	Difference of Logits Ratio Loss	when	Dataset = NSL-KDD	$<1 \times 10^{-5}$	57 %	35 %
9.	<i>Random-Restart: Disabled</i>	is better than	<i>Random-Restart: Enabled</i>	when	Dataset = UNSW-NB15	$<1 \times 10^{-5}$	65 %	33 %
10.	Carlini-Wagner Loss	is better than	Difference of Logits Ratio Loss	when	Dataset = CIFAR-10	$<2.2 \times 10^{-308}$	81 %	32 %
11.	Cross-Entropy	is better than	Carlini-Wagner Loss	when	SaliencyMap = Identity Saliency Map	$<2.2 \times 10^{-308}$	83 %	31 %
12.	Cross-Entropy	is better than	Difference of Logits Ratio Loss	when	Dataset = NSL-KDD	$6.4 \times 10^{-5}$	55 %	31 %
13.	Cross-Entropy	is better than	Identity Loss	when	SaliencyMap = Identity Saliency Map	$<1 \times 10^{-5}$	57 %	30 %
14.	Identity Saliency Map	is better than	DeepFool Saliency Map	when	Loss = Cross-Entropy	$<2.2 \times 10^{-308}$	79 %	30 %
15.	Identity Saliency Map	is better than	Jacobian Saliency Map	when	Dataset = CIFAR-10	$<2.2 \times 10^{-308}$	79 %	29 %

Table 4: The top 15 hypotheses for robust models. Delta represents the difference in effect size when changing to a robust model.

## 6 Discussion

**Domain Constraints.** While adversarial machine learning research has been cast predominantly through images, the threats imposed to machine-learning-based detection systems via malware or network attacks are increasingly concerning. However, producing legitimate adversarial examples in the form of binaries or packet captures is a nuanced process; there are constraints, dictated by the domain, that adversarial examples must comply with [1, 9, 17, 26, 34, 34, 48, 56, 59].

In addition, adversarial goals in such domains are not precisely captured by Equation 1; attacks are commonly *targeted* towards a specific class (such as, classifying a variety of malicious network flows as benign traffic [31, 48, 49, 59] or malware families as legitimate software [1, 16, 17, 23, 27]). Moreover, recent work has shown the unique challenges of producing adversarial examples in the *problem space* [16, 17, 41]. Such works identified a set of properties input perturbations must adhere to in order to be considered demonstrative of malicious inputs in the respective problem space (e.g., packet captures or binaries), such as semantic preservation, problem-space transformations, robustness to preprocessing, among other important attributes.

These necessary factors provide a more realistic perspective on the robustness of machine learning systems in security-critical domains. While we did not explore these factors for scope, we acknowledge their importance, and encourage subsequent investigations to incorporate these factors (such as ensuring perturbations are constraint-compliant at the  $\ell_p$  layer of surfaces or adapting loss functions to ensure adversarial examples are misclassified as a specific target class).

**The Threat Landscape.** *White-box* adversaries are important because they represent worst-case failure modes of machine learning systems. However, *black-box* adversaries have demonstrated remarkable efficacy within their limited amount of available knowledge (i.e., practical threats) [4, 25, 38, 52]. While this initial application of our framework focused on white-box adversaries for their prevalence in research, we note that there natural extensions to support black-box adversaries, such as using Backward Pass Differentiable

Approximation [2] in place of the model Jacobian, or the Jacobian-based dataset augmentation [37] as a saliency map for training substitute models, among other techniques. As there are a variety of techniques for efficiently mounting black-box attacks (historically through query minimization) [11, 38, 50, 52], we see value in instantiating our framework with black-box components to understand the trade-offs between such techniques.

**Related Work.** A natural limitation of AutoAttack that the ensemble is fixed; while it was designed to be as diverse as possible to common failures of defenses, it may fail on defenses where an expert-designed adaptive attack would succeed. Thus, the Adaptive AutoAttack (A<sup>3</sup>) extension was introduced to combine the efficacy of AutoAttack, while dynamically adapting to new defenses [60]. A<sup>3</sup> frames building adaptive attacks as a search problem, wherein a surrogate model is built and a “backbone” attack (e.g., FGSM, PGD, CW, among others) is greedily selected, paired with a loss function and subroutines (such as *Random-Restart*). A<sup>3</sup> builds upon AutoAttack in that it enables searching through the attack design space to find the most effective adaptive attack. Our work is complementary in that we provide a broad, modular attack space, while A<sup>3</sup> provides an approach for building adaptive attacks dynamically.

## 7 Conclusion

In this paper, we introduced the space of adversarial strategies. We first presented an extensible decomposition of current attacks into their core components. We subsequently constructed 568 previously unexplored attacks by permuting these components. Through this vast attack space, we measured attack optimality via the PEA: a theoretical attack that upper-bounds attack performance. With the PEA, we studied how attack rankings change across datasets, threat models, and robust vs non-robust models. From these rankings, we described the space of hypotheses, wherein we evaluated how component choices conditionally impact attack efficacy. Our investigation revealed that attack performance is highly contextual—certain components can help (or hurt) attack performance when a specific  $\ell_p$ -norm, compute budget, domain,

and even phenomena is considered. The space of adversarial strategies is rich with highly competitive attacks; meaningful evaluations need to consider the myriad of contextual factors that yield performant adversaries.

## 8 Acknowledgements

We would like to thank the anonymous reviewers for their insightful feedback throughout the review cycle. Additionally, we would like to thank Quinn Burke, Yohan Beugin, Rachel King, and Dave Evans for their helpful comments on earlier versions of this paper.

This research was sponsored by the Combat Capabilities Development Command Army Research Laboratory and was accomplished under Cooperative Agreement Number W911NF-13-2-0045 (ARL Cyber Security CRA). The views and conclusions contained in this document are those of the authors and should not be interpreted as representing the official policies, either expressed or implied, of the Combat Capabilities Development Command Army Research Laboratory or the U.S. Government. The U.S. Government is authorized to reproduce and distribute reprints for Government purposes not withstanding any copyright notation here on. This material is based upon work supported by the National Science Foundation under Grant No. CNS-1805310 and the U.S. Army Research Laboratory and the U.S. Army Research Office under Grant No. W911NF-19-1-0374.

## References

- [1] Hyrum S Anderson, Anant Kharkar, and Bobby Filar. Evading Machine Learning Malware Detection. page 6.
- [2] Anish Athalye, Nicholas Carlini, and David Wagner. Obfuscated Gradients Give a False Sense of Security: Circumventing Defenses to Adversarial Examples. In *ICML*, 2018.
- [3] Battista Biggio, Igino Corona, Davide Maiorca, Blaine Nelson, Nedim Šrđić, Pavel Laskov, Giorgio Giacinto, and Fabio Roli. Evasion Attacks against Machine Learning at Test Time. In *Machine Learning and Knowledge Discovery in Databases*, 2013.
- [4] Wieland Brendel, Jonas Rauber, and Matthias Bethge. Decision-based adversarial attacks: Reliable attacks against black-box machine learning models. *arXiv preprint arXiv:1712.04248*, 2017.
- [5] Nicholas Carlini, Guy Katz, Clark Barrett, and David L. Dill. Provably Minimally-Distorted Adversarial Examples, 2017.
- [6] Nicholas Carlini and David Wagner. Adversarial examples are not easily detected: Bypassing ten detection methods. In *Proceedings of the 10th ACM Workshop on Artificial Intelligence and Security*, pages 3–14, 2017.
- [7] Nicholas Carlini and David Wagner. Towards evaluating the robustness of neural networks. In *IEEE S&P*, 2017.
- [8] Tristan Carrier, Princy Victor, Ali Tekeoglu, and Arash Lashkari. Detecting Obfuscated Malware using Memory Feature Engineering. In *ICISSP*, 2022.
- [9] Varun Chandrasekaran, Brian Tang, Nicolas Papernot, Kassem Fawaz, Somesh Jha, and Xi Wu. Rearchitecting Classification Frameworks For Increased Robustness, 2019. \_eprint: 1905.10900.
- [10] Jiyu Chen, David Wang, and Hao Chen. Explore the Transformation Space for Adversarial Images. In *Proceedings of the Tenth ACM Conference on Data and Application Security and Privacy*, 2020.
- [11] Minhao Cheng, Simranjit Singh, Patrick H. Chen, Pin-Yu Chen, Sijia Liu, and Cho-Jui Hsieh. Sign-OPT: A Query-Efficient Hard-label Adversarial Attack. In *ICLR*, 2020.
- [12] Kang Leng Chiew, Choon Lin Tan, KokSheik Wong, Kelvin S.C. Yong, and Wei King Tiong. A new hybrid ensemble feature selection framework for machine learning-based phishing detection system. *Information Sciences*, 2019.
- [13] F. Croce and M. Hein. Minimally distorted Adversarial Examples with a Fast Adaptive Boundary Attack. In *ICML*, 2020.
- [14] Francesco Croce, Maksym Andriushchenko, Vikash Sehwal, Edoardo DeBenedetti, Nicolas Flammarion, Mung Chiang, Prateek Mittal, and Matthias Hein. Robust-Bench: a standardized adversarial robustness benchmark. *arXiv preprint arXiv:2010.09670*, 2020.
- [15] Francesco Croce and Matthias Hein. Reliable evaluation of adversarial robustness with an ensemble of diverse parameter-free attacks. In *ICML*, 2020.
- [16] Luca Demetrio, Battista Biggio, Giovanni Lagorio, Fabio Roli, and Alessandro Armando. Functionality-Preserving Black-Box Optimization of Adversarial Windows Malware. *IEEE Transactions on Information Forensics and Security*, 2021.
- [17] Luca Demetrio, Battista Biggio, and Fabio Roli. Practical Attacks on Machine Learning: A Case Study on Adversarial Windows Malware. *IEEE S&P*, 2022.
- [18] Ambra Demontis, Marco Melis, Maura Pintor, Matthew Jagielski, Battista Biggio, Alina Oprea, Cristina Nita-Rotaru, and Fabio Roli. Why Do Adversarial Attacks

- Transfer? Explaining Transferability of Evasion and Poisoning Attacks. In *USENIX Security Symposium*, 2019.
- [19] Kevin Eykholt, Ivan Evtimov, Earlene Fernandes, Bo Li, Amir Rahmati, Chaowei Xiao, Atul Prakash, Ta-dayoshi Kohno, and Dawn Song. Robust physical-world attacks on deep learning visual classification. In *Proceedings of the IEEE CVPR*, 2018.
- [20] Samuel G Finlayson, John D Bowers, Joichi Ito, Jonathan L Zittrain, Andrew L Beam, and Isaac S Kohane. Adversarial attacks on medical machine learning. *Science*, 2019.
- [21] Heitor M. Gomes, Albert Bifet, Jesse Read, Jean Paul Barddal, Fabrício Enembreck, Bernhard Pfahringer, Geoff Holmes, and Talel Abdesslem. Adaptive Random Forests for Evolving Data Stream Classification. 2017.
- [22] Ian J Goodfellow, Jonathon Shlens, and Christian Szegedy. Explaining and harnessing adversarial examples. *arXiv preprint arXiv:1412.6572*, 2014.
- [23] Kathrin Grosse, Nicolas Papernot, Praveen Manoharan, Michael Backes, and Patrick McDaniel. Adversarial examples for malware detection. In *European Symposium on Research in Computer Security*, 2017.
- [24] Greg Hamerly and Charles Elkan. Alternatives to the k-means algorithm that find better clusterings. In *Proc. of the Int. Conf. on Inf. and Knowledge Manage.*, 2002.
- [25] Andrew Ilyas, Logan Engstrom, Anish Athalye, and Jessy Lin. Black-box adversarial attacks with limited queries and information. *arXiv preprint arXiv:1804.08598*, 2018.
- [26] Lakshya Jain, Varun Chandrasekaran, Uyeong Jang, Wilson Wu, Andrew Lee, Andy Yan, Steven Chen, Somesh Jha, and Sanjit A. Seshia. Analyzing and Improving Neural Networks by Generating Semantic Counterexamples through Differentiable Rendering, 2019.
- [27] Upinder Kaur, Z. Berkay Celik, and Richard M. Voyles. Robust and Energy Efficient Malware Detection for Robotic Cyber-Physical Systems. In *2022 ACM/IEEE 13th International Conference on Cyber-Physical Systems (ICCP)*, pages 314–315, 2022.
- [28] Alex Krizhevsky. Learning multiple layers of features from tiny images. Technical report, 2009.
- [29] Alexey Kurakin, Ian Goodfellow, and Samy Bengio. Adversarial examples in the physical world. *arXiv preprint arXiv:1607.02533*, 2016.
- [30] Y. Lecun, L. Bottou, Y. Bengio, and P. Haffner. Gradient-based learning applied to document recognition. *Proceedings of the IEEE*, 1998.
- [31] Zilong Lin, Yong Shi, and Zhi Xue. *IDSGAN: Generative Adversarial Networks for Attack Generation against Intrusion Detection*. 2018.
- [32] Daniel Lowd and Christopher Meek. Adversarial Learning. In *Proceedings of the Eleventh ACM SIGKDD International Conference on Knowledge Discovery in Data Mining*, 2005.
- [33] Aleksander Madry, Aleksandar Makelov, Ludwig Schmidt, Dimitris Tsipras, and Adrian Vladu. Towards deep learning models resistant to adversarial attacks. *arXiv preprint arXiv:1706.06083*, 2017.
- [34] Stefano Melacci, Gabriele Ciravegna, Angelo Sotgiu, Ambra Demontis, Battista Biggio, Marco Gori, and Fabio Roli. Domain Knowledge Alleviates Adversarial Attacks in Multi-Label Classifiers. *IEEE Transactions on Pattern Analysis and Machine Intelligence*, 2021.
- [35] S. Moosavi-Dezfooli, A. Fawzi, and P. Frossard. DeepFool: A Simple and Accurate Method to Fool Deep Neural Networks. In *2016 IEEE Conference on Computer Vision and Pattern Recognition (CVPR)*, 2016.
- [36] N. Moustafa and J. Slay. UNSW-NB15: a comprehensive data set for network intrusion detection systems (UNSW-NB15 network data set). In *MilCIS*, 2015.
- [37] Nicolas Papernot, Patrick McDaniel, and Ian Goodfellow. *Transferability in Machine Learning: from Phenomena to Black-Box Attacks using Adversarial Samples*. 2016. [\\_eprint: 1605.07277](https://arxiv.org/abs/1605.07277).
- [38] Nicolas Papernot, Patrick McDaniel, Ian Goodfellow, Somesh Jha, Z Berkay Celik, and Ananthram Swami. Practical black-box attacks against machine learning. In *Asia CCS*, 2017.
- [39] Nicolas Papernot, Patrick McDaniel, Somesh Jha, Matt Fredrikson, Z Berkay Celik, and Ananthram Swami. The limitations of deep learning in adversarial settings. In *IEEE EuroS&P*, 2016.
- [40] Adam Paszke, Sam Gross, Francisco Massa, Adam Lerer, James Bradbury, Gregory Chanan, Trevor Killeen, Zeming Lin, Natalia Gimelshein, Luca Antiga, Alban Desmaison, Andreas Kopf, Edward Yang, Zachary DeVito, Martin Raison, Alykhan Tejani, Sasank Chilamkurthy, Benoit Steiner, Lu Fang, Junjie Bai, and Soumith Chintala. PyTorch: An Imperative Style, High-Performance Deep Learning Library. In *Advances in Neural Information Processing Systems 32*. 2019.
- [41] Fabio Pierazzi, Feargus Pendlebury, Jacopo Cortellazzi, and Lorenzo Cavallaro. Intriguing Properties of Adversarial ML Attacks in the Problem Space. In *IEEE Symposium on Security and Privacy*, 2020.

- [42] Kui Ren, Tianhang Zheng, Zhan Qin, and Xue Liu. Adversarial attacks and defenses in deep learning. *Engineering*, 2020.
- [43] Eitan Richardson and Yair Weiss. A bayes-optimal view on adversarial examples. *Journal of Machine Learning Research*, 22(221):1–28, 2021.
- [44] Jérôme Rony, Luiz G. Hafemann, Luiz S. Oliveira, Ismail Ben Ayed, Robert Sabourin, and Eric Granger. Decoupling Direction and Norm for Efficient Gradient-Based L2 Adversarial Attacks and Defenses. In *IEEE CVPR*, 2019.
- [45] Stuart J. Russell and Peter Norvig. *Artificial Intelligence: a modern approach*. Pearson, 3 edition, 2009.
- [46] Ali Shafahi, Mahyar Najibi, Amin Ghiasi, Zheng Xu, John P. Dickerson, Christoph Studer, Larry S. Davis, Gavin Taylor, and Tom Goldstein. Adversarial training for free! In *NeurIPS*, 2019.
- [47] Mahmood Sharif, Lujo Bauer, and Michael Reiter. On the Suitability of Lp-Norms for Creating and Preventing Adversarial Examples. pages 1686–16868, June 2018.
- [48] Ryan Sheatsley, Blaine Hoak, Eric Pauley, Yohan Beugin, Michael J. Weisman, and Patrick McDaniel. On the Robustness of Domain Constraints. In *Proceedings of the 2021 ACM SIGSAC Conference on Computer and Communications Security*, 2021.
- [49] Ryan Sheatsley, Nicolas Papernot, Michael Weisman, Gunjan Verma, and Patrick McDaniel. Adversarial Examples in Constrained Domains. *arXiv:2011.01183 [cs]*, 2020.
- [50] Satya Narayan Shukla, Anit Kumar Sahu, Devin Willmott, and Zico Kolter. Simple and Efficient Hard Label Black-Box Adversarial Attacks in Low Query Budget Regimes. In *Proceedings of the ACM SIGKDD Conference on Knowledge Discovery & Data Mining*, 2021.
- [51] C. Spearman. The Proof and Measurement of Association between Two Things. *The American Journal of Psychology*, 1987.
- [52] Fnu Suya, Jianfeng Chi, David Evans, and Yuan Tian. Hybrid Batch Attacks: Finding black-box adversarial examples with limited queries. In *USENIX Security Symposium*, 2020.
- [53] Christian Szegedy, Wojciech Zaremba, Ilya Sutskever, Joan Bruna, Dumitru Erhan, Ian Goodfellow, and Rob Fergus. *Intriguing properties of neural networks*. 2013. [\\_eprint: 1312.6199](#).
- [54] M. Tavallaei, E. Bagheri, W. Lu, and A. A. Ghorbani. A detailed analysis of the KDD CUP 99 data set. In *2009 IEEE Symposium on Computational Intelligence for Security and Defense Applications*, pages 1–6, 2009.
- [55] Florian Tramèr, Nicolas Papernot, Ian Goodfellow, Dan Boneh, and Patrick McDaniel. The space of transferable adversarial examples. *arXiv:1704.03453*, 2017.
- [56] Adelin Travers, Lorna Licollari, Guanghan Wang, Varun Chandrasekaran, Adam Dziedzic, David Lie, and Nicolas Papernot. On the Exploitability of Audio Machine Learning Pipelines to Surreptitious Adversarial Examples. *CoRR*, abs/2108.02010, 2021. [arXiv: 2108.02010](#).
- [57] Daniël Vos and Sicco Verwer. Robust Optimal Classification Trees Against Adversarial Examples. *CoRR*, 2021.
- [58] Han Xiao, Kashif Rasul, and Roland Vollgraf. Fashion-MNIST: a Novel Image Dataset for Benchmarking Machine Learning Algorithms, 2017.
- [59] K. Yang, J. Liu, C. Zhang, and Y. Fang. Adversarial Examples Against the Deep Learning Based Network Intrusion Detection Systems. In *MILCOM*, 2018.
- [60] Chengyuan Yao, Pavol Bielek, Petar Tsankov, and Martin Vechev. Automated Discovery of Adaptive Attacks on Adversarial Defenses. In *NeurIPS*, 2021.
- [61] Richard Zhang, Phillip Isola, Alexei A Efros, Eli Shechtman, and Oliver Wang. The Unreasonable Effectiveness of Deep Features as a Perceptual Metric. In *CVPR*, 2018.
- [62] Tianhang Zheng, Changyou Chen, and Kui Ren. In *Proceedings of the Thirty-Third AAAI Conference on Artificial Intelligence*, 2019.



# A Attack Encoding

Here we provide Table 5 for translating attack numbers to component values.

ATK#	Opt.	CoV	RR	$\ell_p$	SM	Loss	ATK#	Opt.	CoV	RR	$\ell_p$	SM	Loss	ATK#	Opt.	CoV	RR	$\ell_p$	SM	Loss
0	SGD	False	False	$\ell_0$	SM <sub>1</sub>	IL	96	SGD	False	True	$\ell_0$	SM <sub>0</sub>	CWL	192	Adam	True	False	$\ell_0$	SM <sub>1</sub>	CE
1	SGD	False	False	$\ell_2$	SM <sub>1</sub>	IL	97	SGD	False	True	$\ell_2$	SM <sub>0</sub>	CWL	193	Adam	True	False	$\ell_2$	SM <sub>1</sub>	CE
2	SGD	False	False	$\ell_\infty$	SM <sub>1</sub>	IL	98	SGD	False	True	$\ell_\infty$	SM <sub>0</sub>	CWL	194	Adam	True	False	$\ell_\infty$	SM <sub>1</sub>	CE
JSMA	SGD	False	False	$\ell_0$	SM <sub>1</sub>	IL	99	SGD	False	True	$\ell_0$	SM <sub>1</sub>	DLR	195	Adam	True	False	$\ell_0$	SM <sub>0</sub>	CE
4	SGD	False	False	$\ell_2$	SM <sub>1</sub>	IL	100	SGD	False	True	$\ell_2$	SM <sub>1</sub>	DLR	196	Adam	True	False	$\ell_2$	SM <sub>0</sub>	CE
5	SGD	False	False	$\ell_\infty$	SM <sub>1</sub>	IL	101	SGD	False	True	$\ell_\infty$	SM <sub>1</sub>	DLR	197	Adam	True	False	$\ell_\infty$	SM <sub>0</sub>	CE
6	SGD	False	False	$\ell_0$	SM <sub>0</sub>	IL	102	SGD	False	True	$\ell_0$	SM <sub>1</sub>	DLR	198	Adam	True	False	$\ell_0$	SM <sub>1</sub>	CWL
DF	SGD	False	False	$\ell_2$	SM <sub>0</sub>	IL	103	SGD	False	True	$\ell_2$	SM <sub>1</sub>	DLR	199	Adam	True	False	$\ell_2$	SM <sub>1</sub>	CWL
8	SGD	False	False	$\ell_\infty$	SM <sub>0</sub>	IL	104	SGD	False	True	$\ell_\infty$	SM <sub>1</sub>	DLR	200	Adam	True	False	$\ell_\infty$	SM <sub>1</sub>	CWL
9	SGD	False	False	$\ell_0$	SM <sub>1</sub>	CE	105	SGD	False	True	$\ell_0$	SM <sub>0</sub>	DLR	201	Adam	True	False	$\ell_0$	SM <sub>1</sub>	CWL
10	SGD	False	False	$\ell_2$	SM <sub>1</sub>	CE	106	SGD	False	True	$\ell_2$	SM <sub>0</sub>	DLR	202	Adam	True	False	$\ell_2$	SM <sub>1</sub>	CWL
BLM	SGD	False	False	$\ell_\infty$	SM <sub>1</sub>	CE	107	SGD	False	True	$\ell_\infty$	SM <sub>0</sub>	DLR	203	Adam	True	False	$\ell_\infty$	SM <sub>1</sub>	CWL
12	SGD	False	False	$\ell_0$	SM <sub>1</sub>	CE	108	SGD	True	True	$\ell_0$	SM <sub>1</sub>	IL	204	Adam	True	False	$\ell_0$	SM <sub>0</sub>	CWL
13	SGD	False	False	$\ell_2$	SM <sub>1</sub>	CE	109	SGD	True	True	$\ell_2$	SM <sub>1</sub>	IL	205	Adam	True	False	$\ell_2$	SM <sub>0</sub>	CWL
14	SGD	False	False	$\ell_\infty$	SM <sub>1</sub>	CE	110	SGD	True	True	$\ell_\infty$	SM <sub>1</sub>	IL	206	Adam	True	False	$\ell_\infty$	SM <sub>0</sub>	CWL
15	SGD	False	False	$\ell_0$	SM <sub>0</sub>	CE	111	SGD	True	True	$\ell_0$	SM <sub>1</sub>	IL	207	Adam	True	False	$\ell_0$	SM <sub>1</sub>	DLR
16	SGD	False	False	$\ell_2$	SM <sub>0</sub>	CE	112	SGD	True	True	$\ell_2$	SM <sub>1</sub>	IL	208	Adam	True	False	$\ell_2$	SM <sub>1</sub>	DLR
17	SGD	False	False	$\ell_\infty$	SM <sub>0</sub>	CE	113	SGD	True	True	$\ell_\infty$	SM <sub>1</sub>	IL	209	Adam	True	False	$\ell_\infty$	SM <sub>1</sub>	DLR
18	SGD	False	False	$\ell_0$	SM <sub>1</sub>	CWL	114	SGD	True	True	$\ell_0$	SM <sub>0</sub>	IL	210	Adam	True	False	$\ell_0$	SM <sub>1</sub>	DLR
19	SGD	False	False	$\ell_2$	SM <sub>1</sub>	CWL	115	SGD	True	True	$\ell_2$	SM <sub>0</sub>	IL	211	Adam	True	False	$\ell_2$	SM <sub>1</sub>	DLR
20	SGD	False	False	$\ell_\infty$	SM <sub>1</sub>	CWL	116	SGD	True	True	$\ell_\infty$	SM <sub>0</sub>	IL	212	Adam	True	False	$\ell_\infty$	SM <sub>1</sub>	DLR
21	SGD	False	False	$\ell_0$	SM <sub>1</sub>	CWL	117	SGD	True	True	$\ell_0$	SM <sub>1</sub>	CE	213	Adam	True	False	$\ell_0$	SM <sub>0</sub>	DLR
22	SGD	False	False	$\ell_2$	SM <sub>1</sub>	CWL	118	SGD	True	True	$\ell_2$	SM <sub>1</sub>	CE	214	Adam	True	False	$\ell_2$	SM <sub>0</sub>	DLR
23	SGD	False	False	$\ell_\infty$	SM <sub>1</sub>	CWL	119	SGD	True	True	$\ell_\infty$	SM <sub>1</sub>	CE	215	Adam	True	False	$\ell_\infty$	SM <sub>0</sub>	DLR
24	SGD	False	False	$\ell_0$	SM <sub>0</sub>	CWL	120	SGD	True	True	$\ell_0$	SM <sub>1</sub>	CE	216	Adam	False	True	$\ell_0$	SM <sub>1</sub>	IL
25	SGD	False	False	$\ell_2$	SM <sub>0</sub>	CWL	121	SGD	True	True	$\ell_2$	SM <sub>1</sub>	CE	217	Adam	False	True	$\ell_2$	SM <sub>1</sub>	IL
26	SGD	False	False	$\ell_\infty$	SM <sub>0</sub>	CWL	122	SGD	True	True	$\ell_\infty$	SM <sub>1</sub>	CE	218	Adam	False	True	$\ell_\infty$	SM <sub>1</sub>	IL
27	SGD	False	False	$\ell_0$	SM <sub>1</sub>	DLR	123	SGD	True	True	$\ell_0$	SM <sub>0</sub>	CE	219	Adam	False	True	$\ell_0$	SM <sub>1</sub>	IL
28	SGD	False	False	$\ell_2$	SM <sub>1</sub>	DLR	124	SGD	True	True	$\ell_2$	SM <sub>0</sub>	CE	220	Adam	False	True	$\ell_2$	SM <sub>1</sub>	IL
29	SGD	False	False	$\ell_\infty$	SM <sub>1</sub>	DLR	125	SGD	True	True	$\ell_\infty$	SM <sub>0</sub>	CE	221	Adam	False	True	$\ell_\infty$	SM <sub>1</sub>	IL
30	SGD	False	False	$\ell_0$	SM <sub>1</sub>	DLR	126	SGD	True	True	$\ell_0$	SM <sub>1</sub>	CWL	222	Adam	False	True	$\ell_0$	SM <sub>0</sub>	IL
31	SGD	False	False	$\ell_2$	SM <sub>1</sub>	DLR	127	SGD	True	True	$\ell_2$	SM <sub>1</sub>	CWL	223	Adam	False	True	$\ell_2$	SM <sub>0</sub>	IL
32	SGD	False	False	$\ell_\infty$	SM <sub>1</sub>	DLR	128	SGD	True	True	$\ell_\infty$	SM <sub>1</sub>	CWL	224	Adam	False	True	$\ell_\infty$	SM <sub>0</sub>	IL
33	SGD	False	False	$\ell_0$	SM <sub>0</sub>	DLR	129	SGD	True	True	$\ell_0$	SM <sub>1</sub>	CWL	225	Adam	False	True	$\ell_0$	SM <sub>1</sub>	CE
34	SGD	False	False	$\ell_2$	SM <sub>0</sub>	DLR	130	SGD	True	True	$\ell_2$	SM <sub>1</sub>	CWL	226	Adam	False	True	$\ell_2$	SM <sub>1</sub>	CE
35	SGD	False	False	$\ell_\infty$	SM <sub>0</sub>	DLR	131	SGD	True	True	$\ell_\infty$	SM <sub>1</sub>	CWL	227	Adam	False	True	$\ell_\infty$	SM <sub>1</sub>	CE
36	SGD	True	False	$\ell_0$	SM <sub>1</sub>	IL	132	SGD	True	True	$\ell_0$	SM <sub>0</sub>	CWL	228	Adam	False	True	$\ell_0$	SM <sub>1</sub>	CE
37	SGD	True	False	$\ell_2$	SM <sub>1</sub>	IL	133	SGD	True	True	$\ell_2$	SM <sub>0</sub>	CWL	229	Adam	False	True	$\ell_2$	SM <sub>1</sub>	CE
38	SGD	True	False	$\ell_\infty$	SM <sub>1</sub>	IL	134	SGD	True	True	$\ell_\infty$	SM <sub>0</sub>	CWL	230	Adam	False	True	$\ell_\infty$	SM <sub>1</sub>	CE
39	SGD	True	False	$\ell_0$	SM <sub>1</sub>	IL	135	SGD	True	True	$\ell_0$	SM <sub>1</sub>	DLR	231	Adam	False	True	$\ell_0$	SM <sub>0</sub>	CE
40	SGD	True	False	$\ell_2$	SM <sub>1</sub>	IL	136	SGD	True	True	$\ell_2$	SM <sub>1</sub>	DLR	232	Adam	False	True	$\ell_2$	SM <sub>0</sub>	CE
41	SGD	True	False	$\ell_\infty$	SM <sub>1</sub>	IL	137	SGD	True	True	$\ell_\infty$	SM <sub>1</sub>	DLR	233	Adam	False	True	$\ell_\infty$	SM <sub>0</sub>	CE
42	SGD	True	False	$\ell_0$	SM <sub>0</sub>	IL	138	SGD	True	True	$\ell_0$	SM <sub>1</sub>	DLR	234	Adam	False	True	$\ell_0$	SM <sub>1</sub>	CWL
43	SGD	True	False	$\ell_2$	SM <sub>0</sub>	IL	139	SGD	True	True	$\ell_2$	SM <sub>1</sub>	DLR	235	Adam	False	True	$\ell_2$	SM <sub>1</sub>	CWL
44	SGD	True	False	$\ell_\infty$	SM <sub>0</sub>	IL	140	SGD	True	True	$\ell_\infty$	SM <sub>1</sub>	DLR	236	Adam	False	True	$\ell_\infty$	SM <sub>1</sub>	CWL
45	SGD	True	False	$\ell_0$	SM <sub>1</sub>	CE	141	SGD	True	True	$\ell_0$	SM <sub>0</sub>	DLR	237	Adam	False	True	$\ell_0$	SM <sub>1</sub>	CWL
46	SGD	True	False	$\ell_2$	SM <sub>1</sub>	CE	142	SGD	True	True	$\ell_2$	SM <sub>0</sub>	DLR	238	Adam	False	True	$\ell_2$	SM <sub>1</sub>	CWL
47	SGD	True	False	$\ell_\infty$	SM <sub>1</sub>	CE	143	SGD	True	True	$\ell_\infty$	SM <sub>0</sub>	DLR	239	Adam	False	True	$\ell_\infty$	SM <sub>1</sub>	CWL
48	SGD	True	False	$\ell_0$	SM <sub>1</sub>	CE	144	Adam	False	False	$\ell_0$	SM <sub>1</sub>	IL	240	Adam	False	True	$\ell_0$	SM <sub>0</sub>	CWL
49	SGD	True	False	$\ell_2$	SM <sub>1</sub>	CE	145	Adam	False	False	$\ell_2$	SM <sub>1</sub>	IL	241	Adam	False	True	$\ell_2$	SM <sub>0</sub>	CWL
50	SGD	True	False	$\ell_\infty$	SM <sub>1</sub>	CE	146	Adam	False	False	$\ell_\infty$	SM <sub>1</sub>	IL	242	Adam	False	True	$\ell_\infty$	SM <sub>0</sub>	CWL
51	SGD	True	False	$\ell_0$	SM <sub>0</sub>	CE	147	Adam	False	False	$\ell_0$	SM <sub>1</sub>	IL	243	Adam	False	True	$\ell_0$	SM <sub>1</sub>	DLR
52	SGD	True	False	$\ell_2$	SM <sub>0</sub>	CE	148	Adam	False	False	$\ell_2$	SM <sub>1</sub>	IL	244	Adam	False	True	$\ell_2$	SM <sub>1</sub>	DLR
53	SGD	True	False	$\ell_\infty$	SM <sub>0</sub>	CE	149	Adam	False	False	$\ell_\infty$	SM <sub>1</sub>	IL	245	Adam	False	True	$\ell_\infty$	SM <sub>1</sub>	DLR
54	SGD	True	False	$\ell_0$	SM <sub>1</sub>	CWL	150	Adam	False	False	$\ell_0$	SM <sub>1</sub>	IL	246	Adam	False	True	$\ell_0$	SM <sub>1</sub>	DLR
55	SGD	True	False	$\ell_2$	SM <sub>1</sub>	CWL	151	Adam	False	False	$\ell_2$	SM <sub>0</sub>	IL	247	Adam	False	True	$\ell_2$	SM <sub>1</sub>	DLR
56	SGD	True	False	$\ell_\infty$	SM <sub>1</sub>	CWL	152	Adam	False	False	$\ell_\infty$	SM <sub>0</sub>	IL	248	Adam	False	True	$\ell_\infty$	SM <sub>1</sub>	DLR
57	SGD	True	False	$\ell_0$	SM <sub>1</sub>	CWL	153	Adam	False	False	$\ell_0$	SM <sub>1</sub>	CE	249	Adam	False	True	$\ell_0$	SM <sub>0</sub>	DLR
58	SGD	True	False	$\ell_2$	SM <sub>1</sub>	CWL	154	Adam	False	False	$\ell_2$	SM <sub>1</sub>	CE	250	Adam	False	True	$\ell_2$	SM <sub>0</sub>	DLR
59	SGD	True	False	$\ell_\infty$	SM <sub>1</sub>	CWL	155	Adam	False	False	$\ell_\infty$	SM <sub>1</sub>	CE	251	Adam	False	True	$\ell_\infty$	SM <sub>0</sub>	DLR
60	SGD	True	False	$\ell_0$	SM <sub>0</sub>	CWL	156	Adam	False	False	$\ell_0$	SM <sub>1</sub>	CE	252	Adam	True	True	$\ell_0$	SM <sub>1</sub>	IL
61	SGD	True	False	$\ell_2$	SM <sub>0</sub>	CWL	157	Adam	False	False	$\ell_2$	SM <sub>1</sub>	CE	253	Adam	True	True	$\ell_2$	SM <sub>1</sub>	IL
62	SGD	True	False	$\ell_\infty$	SM <sub>0</sub>	CWL	158	Adam	False	False	$\ell_\infty$	SM <sub>1</sub>	CE	254	Adam	True	True	$\ell_\infty$	SM <sub>1</sub>	IL
63	SGD	True	False	$\ell_0$	SM <sub>1</sub>	DLR	159	Adam	False	False	$\ell_0$	SM <sub>0</sub>	CE	255	Adam	True	True	$\ell_0$	SM <sub>1</sub>	IL
64	SGD	True	False	$\ell_2$	SM <sub>1</sub>	DLR	160	Adam	False	False	$\ell_2$	SM <sub>0</sub>	CE	256	Adam	True	True	$\ell_2$	SM <sub>1</sub>	IL
65	SGD	True	False	$\ell_\infty$	SM <sub>1</sub>	DLR	161	Adam	False	False	$\ell_\infty$	SM <sub>0</sub>	CE	257	Adam	True	True	$\ell_\infty$	SM <sub>1</sub>	IL
66	SGD	True	False	$\ell_0$	SM <sub>1</sub>	DLR	162	Adam	False	False	$\ell_0$	SM <sub>1</sub>	CWL	258	Adam	True	True	$\ell_0$	SM <sub>0</sub>	IL
67	SGD	True	False	$\ell_2$	SM <sub>1</sub>	DLR	163	Adam	False	False	$\ell_2$	SM <sub>1</sub>	CWL	259	Adam	True	True	$\ell_2$	SM <sub>0</sub>	IL
68	SGD	True	False	$\ell_\infty$	SM <sub>1</sub>	DLR	164	Adam	False	False	$\ell_\infty$	SM <sub>1</sub>	CWL	260	Adam	True	True	$\ell_\infty$		

ATK#	Opt.	CoV	RR	$\ell_p$	SM	Loss	ATK#	Opt.	CoV	RR	$\ell_p$	SM	Loss	ATK#	Opt.	CoV	RR	$\ell_p$	SM	Loss
288	BWSGD	False	False	$\ell_0$	SM <sub>1</sub>	IL	384	BWSGD	False	True	$\ell_0$	SM <sub>0</sub>	CWL	480	MBS	True	False	$\ell_0$	SM <sub>3</sub>	CE
289	BWSGD	False	False	$\ell_2$	SM <sub>1</sub>	IL	385	BWSGD	False	True	$\ell_2$	SM <sub>0</sub>	CWL	481	MBS	True	False	$\ell_2$	SM <sub>3</sub>	CE
290	BWSGD	False	False	$\ell_{\infty}$	SM <sub>1</sub>	IL	386	BWSGD	False	True	$\ell_{\infty}$	SM <sub>0</sub>	CWL	482	MBS	True	False	$\ell_{\infty}$	SM <sub>3</sub>	CE
291	BWSGD	False	False	$\ell_0$	SM <sub>1</sub>	IL	387	BWSGD	False	True	$\ell_0$	SM <sub>1</sub>	DLR	483	MBS	True	False	$\ell_0$	SM <sub>0</sub>	CE
292	BWSGD	False	False	$\ell_2$	SM <sub>1</sub>	IL	388	BWSGD	False	True	$\ell_2$	SM <sub>1</sub>	DLR	484	MBS	True	False	$\ell_2$	SM <sub>0</sub>	CE
293	BWSGD	False	False	$\ell_{\infty}$	SM <sub>1</sub>	IL	389	BWSGD	False	True	$\ell_{\infty}$	SM <sub>1</sub>	DLR	485	MBS	True	False	$\ell_{\infty}$	SM <sub>0</sub>	CE
294	BWSGD	False	False	$\ell_0$	SM <sub>0</sub>	IL	390	BWSGD	False	True	$\ell_0$	SM <sub>3</sub>	DLR	486	MBS	True	False	$\ell_0$	SM <sub>1</sub>	CWL
FAB	BWSGD	False	False	$\ell_2$	SM <sub>0</sub>	IL	391	BWSGD	False	True	$\ell_2$	SM <sub>3</sub>	DLR	487	MBS	True	False	$\ell_2$	SM <sub>1</sub>	CWL
296	BWSGD	False	False	$\ell_{\infty}$	SM <sub>0</sub>	IL	392	BWSGD	False	True	$\ell_{\infty}$	SM <sub>3</sub>	DLR	488	MBS	True	False	$\ell_{\infty}$	SM <sub>1</sub>	CWL
297	BWSGD	False	False	$\ell_0$	SM <sub>1</sub>	CE	393	BWSGD	False	True	$\ell_0$	SM <sub>0</sub>	DLR	489	MBS	True	False	$\ell_0$	SM <sub>3</sub>	CWL
298	BWSGD	False	False	$\ell_2$	SM <sub>1</sub>	CE	394	BWSGD	False	True	$\ell_2$	SM <sub>0</sub>	DLR	490	MBS	True	False	$\ell_2$	SM <sub>3</sub>	CWL
299	BWSGD	False	False	$\ell_{\infty}$	SM <sub>1</sub>	CE	395	BWSGD	False	True	$\ell_{\infty}$	SM <sub>0</sub>	DLR	491	MBS	True	False	$\ell_{\infty}$	SM <sub>3</sub>	CWL
300	BWSGD	False	False	$\ell_0$	SM <sub>1</sub>	CE	396	BWSGD	True	True	$\ell_0$	SM <sub>1</sub>	IL	492	MBS	True	False	$\ell_0$	SM <sub>0</sub>	CWL
301	BWSGD	False	False	$\ell_2$	SM <sub>1</sub>	CE	397	BWSGD	True	True	$\ell_2$	SM <sub>1</sub>	IL	493	MBS	True	False	$\ell_2$	SM <sub>0</sub>	CWL
302	BWSGD	False	False	$\ell_{\infty}$	SM <sub>1</sub>	CE	398	BWSGD	True	True	$\ell_{\infty}$	SM <sub>1</sub>	IL	494	MBS	True	False	$\ell_{\infty}$	SM <sub>0</sub>	CWL
303	BWSGD	False	False	$\ell_0$	SM <sub>0</sub>	CE	399	BWSGD	True	True	$\ell_0$	SM <sub>3</sub>	IL	495	MBS	True	False	$\ell_0$	SM <sub>1</sub>	DLR
304	BWSGD	False	False	$\ell_2$	SM <sub>0</sub>	CE	400	BWSGD	True	True	$\ell_2$	SM <sub>3</sub>	IL	496	MBS	True	False	$\ell_2$	SM <sub>1</sub>	DLR
305	BWSGD	False	False	$\ell_{\infty}$	SM <sub>0</sub>	CE	401	BWSGD	True	True	$\ell_{\infty}$	SM <sub>3</sub>	IL	497	MBS	True	False	$\ell_{\infty}$	SM <sub>1</sub>	DLR
306	BWSGD	False	False	$\ell_0$	SM <sub>1</sub>	CWL	402	BWSGD	True	True	$\ell_0$	SM <sub>0</sub>	IL	498	MBS	True	False	$\ell_0$	SM <sub>3</sub>	DLR
307	BWSGD	False	False	$\ell_2$	SM <sub>1</sub>	CWL	403	BWSGD	True	True	$\ell_2$	SM <sub>0</sub>	IL	499	MBS	True	False	$\ell_2$	SM <sub>3</sub>	DLR
308	BWSGD	False	False	$\ell_{\infty}$	SM <sub>1</sub>	CWL	404	BWSGD	True	True	$\ell_{\infty}$	SM <sub>0</sub>	IL	500	MBS	True	False	$\ell_{\infty}$	SM <sub>3</sub>	DLR
309	BWSGD	False	False	$\ell_0$	SM <sub>3</sub>	CWL	405	BWSGD	True	True	$\ell_0$	SM <sub>1</sub>	CE	501	MBS	True	False	$\ell_0$	SM <sub>0</sub>	DLR
310	BWSGD	False	False	$\ell_2$	SM <sub>3</sub>	CWL	406	BWSGD	True	True	$\ell_2$	SM <sub>1</sub>	CE	502	MBS	True	False	$\ell_2$	SM <sub>0</sub>	DLR
311	BWSGD	False	False	$\ell_{\infty}$	SM <sub>3</sub>	CWL	407	BWSGD	True	True	$\ell_{\infty}$	SM <sub>1</sub>	CE	503	MBS	True	False	$\ell_{\infty}$	SM <sub>0</sub>	DLR
312	BWSGD	False	False	$\ell_0$	SM <sub>0</sub>	CWL	408	BWSGD	True	True	$\ell_0$	SM <sub>1</sub>	CE	504	MBS	False	True	$\ell_0$	SM <sub>1</sub>	IL
313	BWSGD	False	False	$\ell_2$	SM <sub>0</sub>	CWL	409	BWSGD	True	True	$\ell_2$	SM <sub>1</sub>	CE	505	MBS	False	True	$\ell_2$	SM <sub>1</sub>	IL
314	BWSGD	False	False	$\ell_{\infty}$	SM <sub>0</sub>	CWL	410	BWSGD	True	True	$\ell_{\infty}$	SM <sub>1</sub>	CE	506	MBS	False	True	$\ell_{\infty}$	SM <sub>1</sub>	IL
315	BWSGD	False	False	$\ell_0$	SM <sub>1</sub>	DLR	411	BWSGD	True	True	$\ell_0$	SM <sub>0</sub>	CE	507	MBS	False	True	$\ell_0$	SM <sub>1</sub>	IL
316	BWSGD	False	False	$\ell_2$	SM <sub>1</sub>	DLR	412	BWSGD	True	True	$\ell_2$	SM <sub>0</sub>	CE	508	MBS	False	True	$\ell_2$	SM <sub>1</sub>	IL
317	BWSGD	False	False	$\ell_{\infty}$	SM <sub>1</sub>	DLR	413	BWSGD	True	True	$\ell_{\infty}$	SM <sub>0</sub>	CE	509	MBS	False	True	$\ell_{\infty}$	SM <sub>1</sub>	IL
318	BWSGD	False	False	$\ell_0$	SM <sub>1</sub>	DLR	414	BWSGD	True	True	$\ell_0$	SM <sub>1</sub>	CWL	510	MBS	False	True	$\ell_0$	SM <sub>0</sub>	IL
319	BWSGD	False	False	$\ell_2$	SM <sub>1</sub>	DLR	415	BWSGD	True	True	$\ell_2$	SM <sub>1</sub>	CWL	511	MBS	False	True	$\ell_2$	SM <sub>0</sub>	IL
320	BWSGD	False	False	$\ell_{\infty}$	SM <sub>1</sub>	DLR	416	BWSGD	True	True	$\ell_{\infty}$	SM <sub>1</sub>	CWL	512	MBS	False	True	$\ell_{\infty}$	SM <sub>0</sub>	IL
321	BWSGD	False	False	$\ell_0$	SM <sub>0</sub>	DLR	417	BWSGD	True	True	$\ell_0$	SM <sub>3</sub>	CWL	513	MBS	False	True	$\ell_0$	SM <sub>1</sub>	CE
322	BWSGD	False	False	$\ell_2$	SM <sub>0</sub>	DLR	418	BWSGD	True	True	$\ell_2$	SM <sub>3</sub>	CWL	514	MBS	False	True	$\ell_2$	SM <sub>1</sub>	CE
323	BWSGD	False	False	$\ell_{\infty}$	SM <sub>0</sub>	DLR	419	BWSGD	True	True	$\ell_{\infty}$	SM <sub>3</sub>	CWL	APGD-CE	MBS	False	True	$\ell_{\infty}$	SM <sub>1</sub>	CE
324	BWSGD	True	False	$\ell_0$	SM <sub>1</sub>	IL	420	BWSGD	True	True	$\ell_0$	SM <sub>0</sub>	CWL	516	MBS	False	True	$\ell_0$	SM <sub>1</sub>	CE
325	BWSGD	True	False	$\ell_2$	SM <sub>1</sub>	IL	421	BWSGD	True	True	$\ell_2$	SM <sub>0</sub>	CWL	517	MBS	False	True	$\ell_2$	SM <sub>1</sub>	CE
326	BWSGD	True	False	$\ell_{\infty}$	SM <sub>1</sub>	IL	422	BWSGD	True	True	$\ell_{\infty}$	SM <sub>0</sub>	CWL	518	MBS	False	True	$\ell_{\infty}$	SM <sub>1</sub>	CE
327	BWSGD	True	False	$\ell_0$	SM <sub>1</sub>	IL	423	BWSGD	True	True	$\ell_0$	SM <sub>1</sub>	DLR	519	MBS	False	True	$\ell_0$	SM <sub>0</sub>	CE
328	BWSGD	True	False	$\ell_2$	SM <sub>1</sub>	IL	424	BWSGD	True	True	$\ell_2$	SM <sub>1</sub>	DLR	520	MBS	False	True	$\ell_2$	SM <sub>0</sub>	CE
329	BWSGD	True	False	$\ell_{\infty}$	SM <sub>1</sub>	IL	425	BWSGD	True	True	$\ell_{\infty}$	SM <sub>1</sub>	DLR	521	MBS	False	True	$\ell_{\infty}$	SM <sub>0</sub>	CE
330	BWSGD	True	False	$\ell_0$	SM <sub>0</sub>	IL	426	BWSGD	True	True	$\ell_0$	SM <sub>3</sub>	DLR	522	MBS	False	True	$\ell_0$	SM <sub>1</sub>	CWL
331	BWSGD	True	False	$\ell_2$	SM <sub>0</sub>	IL	427	BWSGD	True	True	$\ell_2$	SM <sub>3</sub>	DLR	523	MBS	False	True	$\ell_2$	SM <sub>1</sub>	CWL
332	BWSGD	True	False	$\ell_{\infty}$	SM <sub>0</sub>	IL	428	BWSGD	True	True	$\ell_{\infty}$	SM <sub>3</sub>	DLR	524	MBS	False	True	$\ell_{\infty}$	SM <sub>1</sub>	CWL
333	BWSGD	True	False	$\ell_0$	SM <sub>1</sub>	CE	429	BWSGD	True	True	$\ell_0$	SM <sub>0</sub>	DLR	525	MBS	False	True	$\ell_0$	SM <sub>3</sub>	CWL
334	BWSGD	True	False	$\ell_2$	SM <sub>1</sub>	CE	430	BWSGD	True	True	$\ell_2$	SM <sub>0</sub>	DLR	526	MBS	False	True	$\ell_2$	SM <sub>3</sub>	CWL
335	BWSGD	True	False	$\ell_{\infty}$	SM <sub>1</sub>	CE	431	BWSGD	True	True	$\ell_{\infty}$	SM <sub>0</sub>	DLR	527	MBS	False	True	$\ell_{\infty}$	SM <sub>3</sub>	CWL
336	BWSGD	True	False	$\ell_0$	SM <sub>3</sub>	CE	432	MBS	False	False	$\ell_0$	SM <sub>1</sub>	IL	528	MBS	False	True	$\ell_0$	SM <sub>0</sub>	CWL
337	BWSGD	True	False	$\ell_2$	SM <sub>3</sub>	CE	433	MBS	False	False	$\ell_2$	SM <sub>1</sub>	IL	529	MBS	False	True	$\ell_2$	SM <sub>0</sub>	CWL
338	BWSGD	True	False	$\ell_{\infty}$	SM <sub>3</sub>	CE	434	MBS	False	False	$\ell_{\infty}$	SM <sub>1</sub>	IL	530	MBS	False	True	$\ell_{\infty}$	SM <sub>0</sub>	CWL
339	BWSGD	True	False	$\ell_0$	SM <sub>0</sub>	CE	435	MBS	False	False	$\ell_0$	SM <sub>3</sub>	IL	531	MBS	False	True	$\ell_0$	SM <sub>1</sub>	DLR
340	BWSGD	True	False	$\ell_2$	SM <sub>0</sub>	CE	436	MBS	False	False	$\ell_2$	SM <sub>3</sub>	IL	532	MBS	False	True	$\ell_2$	SM <sub>1</sub>	DLR
341	BWSGD	True	False	$\ell_{\infty}$	SM <sub>0</sub>	CE	437	MBS	False	False	$\ell_{\infty}$	SM <sub>3</sub>	IL	APGD-DLR	MBS	False	True	$\ell_{\infty}$	SM <sub>1</sub>	DLR
342	BWSGD	True	False	$\ell_0$	SM <sub>1</sub>	CWL	438	MBS	False	False	$\ell_0$	SM <sub>0</sub>	IL	534	MBS	False	True	$\ell_0$	SM <sub>3</sub>	DLR
343	BWSGD	True	False	$\ell_2$	SM <sub>1</sub>	CWL	439	MBS	False	False	$\ell_2$	SM <sub>0</sub>	IL	535	MBS	False	True	$\ell_2$	SM <sub>3</sub>	DLR
344	BWSGD	True	False	$\ell_{\infty}$	SM <sub>1</sub>	CWL	440	MBS	False	False	$\ell_{\infty}$	SM <sub>0</sub>	IL	536	MBS	False	True	$\ell_{\infty}$	SM <sub>3</sub>	DLR
345	BWSGD	True	False	$\ell_0$	SM <sub>3</sub>	CWL	441	MBS	False	False	$\ell_0$	SM <sub>1</sub>	CE	537	MBS	False	True	$\ell_0$	SM <sub>0</sub>	DLR
346	BWSGD	True	False	$\ell_2$	SM <sub>3</sub>	CWL	442	MBS	False	False	$\ell_2$	SM <sub>1</sub>	CE	538	MBS	False	True	$\ell_2$	SM <sub>0</sub>	DLR
347	BWSGD	True	False	$\ell_{\infty}$	SM <sub>3</sub>	CWL	443	MBS	False	False	$\ell_{\infty}$	SM <sub>1</sub>	CE	539	MBS	False	True	$\ell_{\infty}$	SM <sub>0</sub>	DLR
348	BWSGD	True	False	$\ell_0$	SM <sub>0</sub>	CWL	444	MBS	False	False	$\ell_0$	SM <sub>3</sub>	CE	540	MBS	True	True	$\ell_0$	SM <sub>1</sub>	IL
349	BWSGD	True	False	$\ell_2$	SM <sub>0</sub>	CWL	445	MBS	False	False	$\ell_2$	SM <sub>3</sub>	CE	541	MBS	True	True	$\ell_2$	SM <sub>1</sub>	IL
350	BWSGD	True	False	$\ell_{\infty}$	SM <sub>0</sub>	CWL	446	MBS	False	False	$\ell_{\infty}$	SM <sub>3</sub>	CE	542	MBS	True	True	$\ell_{\infty}$	SM <sub>1</sub>	IL
351	BWSGD	True	False	$\ell_0$	SM <sub>1</sub>	DLR	447	MBS	False	False	$\ell_0$	SM <sub>0</sub>	CE	543	MBS	True	True	$\ell_0$	SM <sub>3</sub>	IL
352	BWSGD	True	False	$\ell_2$	SM <sub>1</sub>	DLR	448	MBS	False	False	$\ell_2$	SM <sub>0</sub>	CE	544	MBS	True	True	$\ell_2$	SM <sub>3</sub>	IL
353	BWSGD	True	False	$\ell_{\infty}$	SM <sub>1</sub>	DLR	449	MBS	False	False	$\ell_{\infty}$	SM <sub>0</sub>	CE	545	MBS	True	True	$\ell_{\infty}$	SM <sub>3</sub>	IL
354	BWSGD	True	False	$\ell_0$	SM <sub>3</sub>	DLR	450	MBS	False	False	$\ell_0$	SM <sub>1</sub>	CWL	546	MBS	True	True	$\ell_0$	SM <sub>0</sub>	IL
355	BWSGD	True	False	$\ell_2$	SM <sub>3</sub>	DLR	451	MBS	False	False	$\ell_2$	SM <sub>1</sub>	CWL	547	MBS	True	True	$\ell_2$	SM <sub>0</sub>	IL
356	BWSGD	True	False	$\ell_{\infty}$	SM <sub>3</sub>	DLR	452	MBS	False	False	$\ell_{\infty}$	SM <sub>1</sub>	CWL							

## B Comparison to Known Attacks

Here we provide the full version of [Table 2](#).

$\ell_0$ Attacks				$\ell_2$ Attacks				$\ell_\infty$ Attacks				$\ell_0$ Attacks				$\ell_2$ Attacks				$\ell_\infty$ Attacks																																																																																																																																																																																																																																																																																																																																																																																																																											
Rank	Attack	% Reduction	$\ell_0$ Budget	Rank	Attack	% Reduction	$\ell_2$ Budget	Rank	Attack	% Reduction	$\ell_\infty$ Budget	Rank	Attack	% Reduction	$\ell_0$ Budget	Rank	Attack	% Reduction	$\ell_2$ Budget	Rank	Attack	% Reduction	$\ell_\infty$ Budget	Rank	Attack	% Reduction	$\ell_2$ Budget	Rank	Attack	% Reduction	$\ell_\infty$ Budget																																																																																																																																																																																																																																																																																																																																																																																																																
1.	ATK <sub>171</sub>	-41%	0.10	1.	ATK <sub>460</sub>	-50%	0.12	1.	ATK <sub>449</sub>	-8%	0.22	97.	ATK <sub>405</sub>	+0%	0.00	97.	ATK <sub>427</sub>	+0%	0.00	97.	ATK <sub>445</sub>	+237%	0.81	98.	ATK <sub>413</sub>	+237%	0.81	98.	ATK <sub>413</sub>	+237%	0.81	99.	ATK <sub>429</sub>	+0%	0.00	100.	ATK <sub>400</sub>	+0%	0.00	100.	ATK <sub>460</sub>	+241%	0.82	101.	ATK <sub>426</sub>	+0%	0.00	101.	ATK <sub>385</sub>	+241%	0.82	102.	ATK <sub>402</sub>	+0%	0.00	102.	ATK <sub>379</sub>	+241%	0.82	103.	ATK <sub>396</sub>	+0%	0.00	103.	ATK <sub>382</sub>	+258%	0.86	104.	ATK <sub>376</sub>	+0%	0.00	104.	ATK <sub>376</sub>	+258%	0.86	105.	ATK <sub>370</sub>	+0%	0.00	106.	ATK <sub>373</sub>	+275%	0.90	107.	ATK <sub>394</sub>	+0%	0.00	108.	ATK <sub>355</sub>	+275%	0.90	109.	ATK <sub>388</sub>	+0%	0.00	109.	ATK <sub>369</sub>	+279%	0.91	110.	ATK <sub>391</sub>	+0%	0.00	111.	ATK <sub>361</sub>	+279%	0.91	112.	ATK <sub>364</sub>	+287%	0.93	113.	ATK <sub>349</sub>	+291%	0.94	114.	ATK <sub>343</sub>	+291%	0.94	115.	ATK <sub>346</sub>	+291%	0.94	116.	ATK <sub>340</sub>	+291%	0.94	117.	ATK <sub>344</sub>	+291%	0.94	118.	ATK <sub>337</sub>	+291%	0.94	119.	ATK <sub>358</sub>	+295%	0.95	120.	ATK <sub>392</sub>	+295%	0.95	121.	ATK <sub>352</sub>	+295%	0.95	122.	ATK <sub>331</sub>	+295%	0.95	123.	ATK <sub>325</sub>	+295%	0.95	124.	ATK <sub>328</sub>	+295%	0.95	125.	ATK <sub>313</sub>	+300%	0.96	126.	ATK <sub>307</sub>	+300%	0.96	127.	ATK <sub>310</sub>	+300%	0.96	128.	ATK <sub>304</sub>	+300%	0.96	129.	ATK <sub>298</sub>	+300%	0.96	130.	ATK <sub>301</sub>	+300%	0.96	131.	ATK <sub>306</sub>	+300%	0.96	132.	ATK <sub>312</sub>	+304%	0.97	133.	ATK <sub>319</sub>	+304%	0.97	134.	ATK <sub>289</sub>	+304%	0.97	135.	ATK <sub>292</sub>	+304%	0.97	136.	DF	+287%	0.91	137.	FAB	+287%	0.91	138.	ATK <sub>299</sub>	+287%	0.91	139.	ATK <sub>288</sub>	+287%	0.91	140.	ATK <sub>291</sub>	+287%	0.91	141.	ATK <sub>293</sub>	+287%	0.91	142.	ATK <sub>294</sub>	+287%	0.91	143.	ATK <sub>295</sub>	+287%	0.91	144.	ATK <sub>296</sub>	+287%	0.91	145.	ATK <sub>297</sub>	+287%	0.91	146.	ATK <sub>298</sub>	+287%	0.91	147.	ATK <sub>299</sub>	+287%	0.91	148.	ATK <sub>300</sub>	+287%	0.91	149.	ATK <sub>301</sub>	+287%	0.91	150.	ATK <sub>302</sub>	+287%	0.91	151.	ATK <sub>303</sub>	+287%	0.91	152.	ATK <sub>304</sub>	+287%	0.91	153.	ATK <sub>305</sub>	+287%	0.91	154.	ATK <sub>306</sub>	+287%	0.91	155.	ATK <sub>307</sub>	+287%	0.91	156.	ATK <sub>308</sub>	+287%	0.91	157.	ATK <sub>309</sub>	+287%	0.91	158.	ATK <sub>310</sub>	+287%	0.91	159.	ATK <sub>311</sub>	+287%	0.91	160.	ATK <sub>312</sub>	+287%	0.91	161.	ATK <sub>313</sub>	+287%	0.91	162.	ATK <sub>314</sub>	+287%	0.91	163.	ATK <sub>315</sub>	+287%	0.91	164.	ATK <sub>316</sub>	+287%	0.91	165.	ATK <sub>317</sub>	+287%	0.91	166.	ATK <sub>318</sub>	+287%	0.91	167.	ATK <sub>319</sub>	+287%	0.91	168.	ATK <sub>320</sub>	+287%	0.91	169.	ATK <sub>321</sub>	+287%	0.91	170.	ATK <sub>322</sub>	+287%	0.91	171.	ATK <sub>323</sub>	+287%	0.91	172.	ATK <sub>324</sub>	+287%	0.91	173.	ATK <sub>325</sub>	+287%	0.91	174.	ATK <sub>326</sub>	+287%	0.91	175.	ATK <sub>327</sub>	+287%	0.91	176.	ATK <sub>328</sub>	+287%	0.91	177.	ATK <sub>329</sub>	+287%	0.91	178.	ATK <sub>330</sub>	+287%	0.91	179.	ATK <sub>331</sub>	+287%	0.91	180.	ATK <sub>332</sub>	+287%	0.91	181.	ATK <sub>333</sub>	+287%	0.91	182.	ATK <sub>334</sub>	+287%	0.91	183.	ATK <sub>335</sub>	+287%	0.91	184.	ATK <sub>336</sub>	+287%	0.91	185.	ATK <sub>337</sub>	+287%	0.91	186.	ATK <sub>338</sub>	+287%	0.91	187.	ATK <sub>339</sub>	+287%	0.91	188.	ATK <sub>340</sub>	+287%	0.91	189.	ATK <sub>341</sub>	+287%	0.91	190.	ATK <sub>342</sub>	+287%	0.91	191.	ATK <sub>343</sub>	+287%	0.91	192.	ATK <sub>344</sub>	+287%	0.91

Table 6: MNIST Relative Attack Comparisons. Budgets are normalized. Attacks that fail to reduce model accuracy to be  $<1\%$  are labeled as consuming infinite budget. Improvements are relative to the best known attack for each  $\ell_p$ -norm.

## C The Optimal Attack

Here, we show the median Spearman rank correlation coefficients for each of our datasets and threat models. For the dataset plots, results are segmented by  $\ell_p$ -norm. Data points correspond to a specific threat model (i.e., a value for  $\theta$ ).  $\theta = \{0.0, 0.5, 1.0, 1.5, 2.0\}$  are labeled for reference. High attack performance generalization is encoded as lighter shades, while low generalization is encoded with darker shades, as shown in the colorbar below:

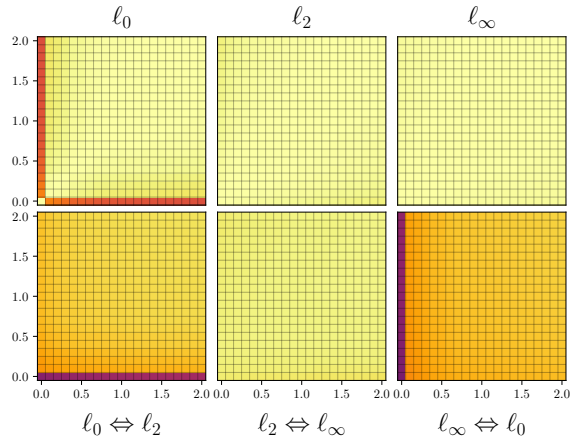


Figure 7: Phishing

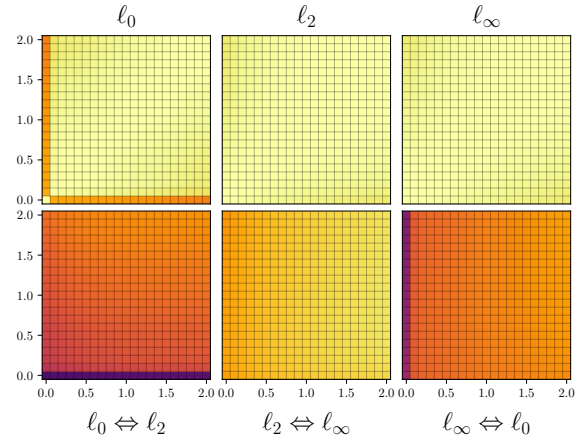


Figure 9: UNSW-NB15

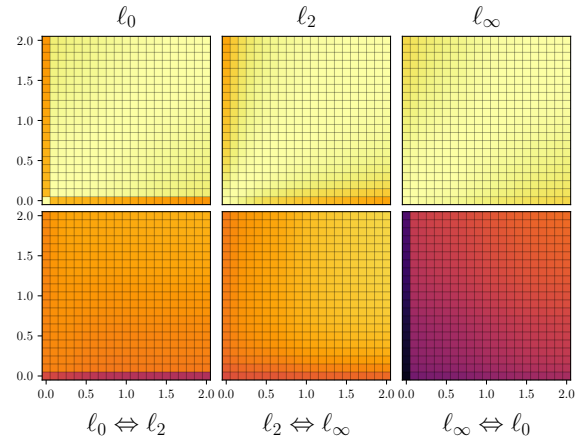


Figure 10: MNIST

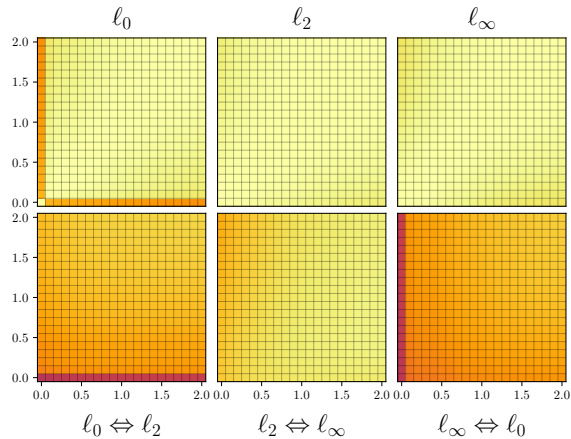


Figure 8: NSL-KDD

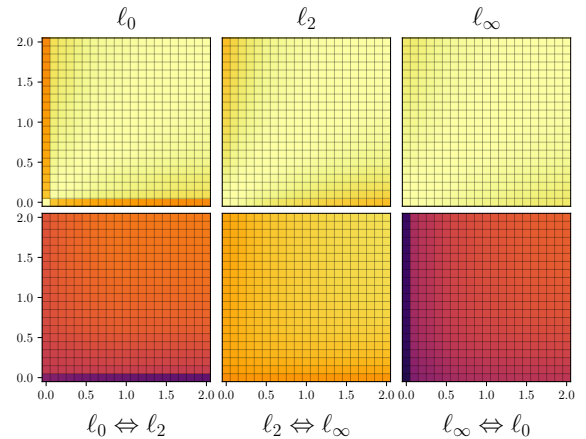


Figure 11: FMNIST

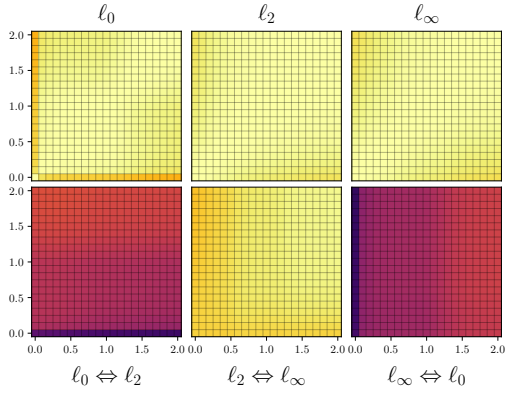


Figure 12: CIFAR-10

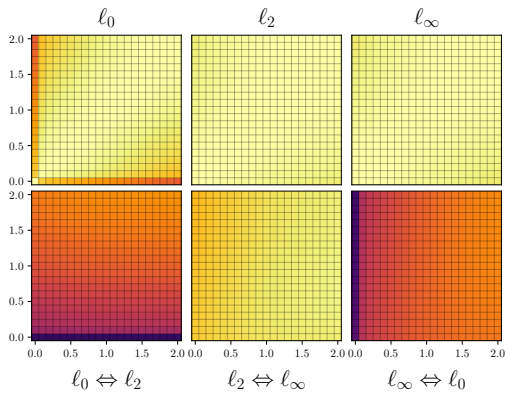
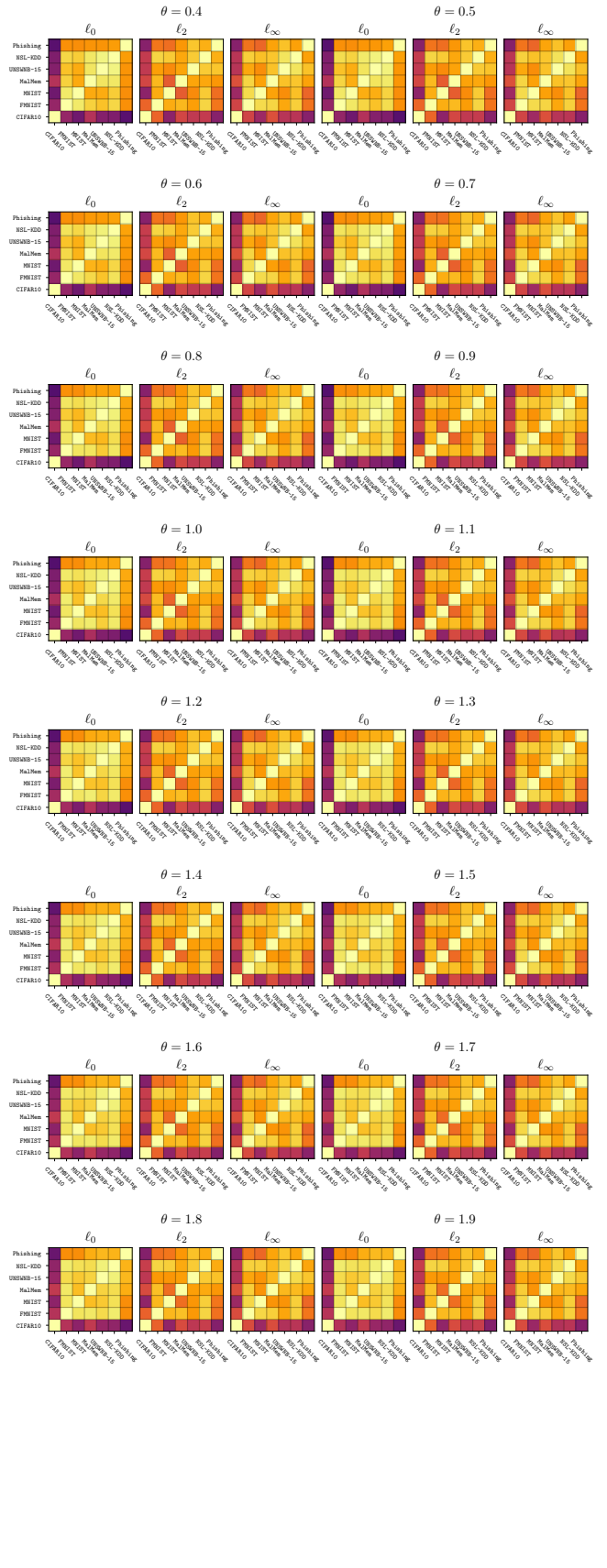


Figure 13: CIC-MalMem-2022



## D Miscellany

**Table 7** provides a listing of model hyperparameters for each of our datasets. Our selection was inspired by publications that report state-of-the-art accuracy for the models we used. **Table 9** provides a listing of all symbols used in this paper and their associated meanings. **Table 8** provides the parameters used for adversarial training.

### D.1 Attack Modifications

**Carlini-Wagner Attack.** As described in [section 3](#), the CW attack loss function includes a hyperparameter  $c$  which controls the trade-off between the distortion introduced and misclassification. In the original attack definition,  $c$  is optimized dynamically through binary-search [7]. This is cost-prohibitive and prevents us from performing any meaningful evaluation when computational cost is considered (as this attack would exist on a separate scale, when compared to PGD or even the JSMA, which requires the model Jacobian). To remedy this, we select a constant value of  $c$  in our experiments. From the investigation on values of  $c$  in [7] with respect to attack success probability versus mean  $\ell_2$  distance, we choose a value of 1.0 for  $c$  in all experiments.

**Jacobian-based Saliency Map Approach.** The original definition of the JSMA included a *search space*, which defined the set of candidate features to be selected for perturbation. In the original publication, the JSMA initially set  $\alpha$  to either 1 or 0 (that is, pixels were fully turned “off” or “on”). We find that this underestimates the performance of the JSMA on many datasets. Instead, we derive a more effective strategy of instead setting the saliency map score for some feature  $i$  (in an input  $x$ ) to 0 if: (1) the saliency score for  $i$  is positive and  $x_i = 1$ , or (2) the saliency score for  $i$  is negative and  $x_i = 0$ . This prevents our version of the JSMA from selecting features that are already at limits of valid feature values (i.e., 1 and 0). Moreover, we do not select pixel pairs, as described in [39], as we found our implementation to be at least as effective (often more) as the original JSMA.

**Difference of Logits Ratio Loss.** The original formulation of DLR requires takes the ratio of the differences

between: (1) the true logit and largest non-true-class logit, and (2) the largest logit and the third largest logit. In our evaluation, we used datasets that had less than three classes. For those scenarios, we take the second largest logit.

	Phishing	NSL-KDD	UNSW-NB15	MNIST	FMNIST	CIFAR-10	MalMem
Conv. Neurons	-	-	-	(16,32)	(16,32)	(3,64,64,128,128,256,256,	-
Kernel Size	-	-	-	3	3	3	-
Stride	-	-	-	1	1	1	-
Dropout Prob.	-	-	-	0.4	0.4	0.5	-
MaxPool Kernel	-	-	-	2	2	2	-
MaxPool Stride	-	-	-	2	2	2	-
Linear Neurons	(15.)	(60,32)	(15.)	(128.)	(512.)	(512.)	(32.)
Activation	ReLU	ReLU	ReLU	ReLU	ReLU	ReLU	ReLU
Loss	CCE	CCE	CCE	CCE	CCE	CCE	CCE
Optimizer	Adam	Adam	Adam	Adam	Adam	SGD	Adam
Learning Rate	1e-2	1e-2	1e-2	1e-3	1e-3	5e-2	1e-2
Epochs	40	4	40	20	20	300	180
Batch size	32	128	128	64	64	128	64

Table 7: Hyperparameters

	Phishing	NSL-KDD	UNSW-NB15	MNIST	FMNIST	CIFAR-10	CIC-MalMem-2022
Attack	PGD	PGD	PGD	PGD	PGD	PGD	PGD
Epochs	10	10	5	30	30	3	10
$\alpha$	0.01	0.01	0.01	0.01	0.01	0.01	0.01
Random Restart	0.05	0.01	0.01	0.1	0.1	0.03	0.01

Table 8: Adversarial Training Hyperparameters

Symbol	Meaning
$x$	original input
$x'$	adversarial example
$\delta$	perturbation added to $x$
$w$	$x$ in tanh space
$f$	victim model
$f(x)$	model logits
$c$	number of classes
$\hat{y}$	true label
$y$	softmax output
$k$	closest class
$L$	loss function
$\alpha$	single-step perturbation magnitude
$\epsilon$	total perturbation
$J$	Jacobian of a model
SM	Saliency Map
$p$	parameter for some $\ell_p$ -norm
$\theta$	time importance parameter
$B$	budget equation
$b$	budget value for a given equation
$\mathcal{A}$	space of attacks

Table 9: Symbol usage and meaning